UC-25
LBL-17910
c.1

Lawrence Berkeley Laboratory
UNIVERSITY OF CALIFORNIA

Materials & Molecular Research Division

RECEIVED
LAWRENCE
BERKELEY LABORATORY
JUL 24 1984
LIBRARY AND
DOCUMENTS SECTION

THE EFFECT OF PRECIPITATED AUSTENITE ON THE FRACTURE OF A FERRITIC CRYOGENIC STEEL

D.R. Frear
(M.S. Thesis)

May 1984

For Reference
Not to be taken from this room

LBL-17910
c.1

Prepared for the U.S. Department of Energy under Contract DE-AC03-76SF00098

DISCLAIMER

This document was prepared as an account of work sponsored by the United States Government. While this document is believed to contain correct information, neither the United States Government nor any agency thereof, nor the Regents of the University of California, nor any of their employees, makes any warranty, express or implied, or assumes any legal responsibility for the accuracy, completeness, or usefulness of any information, apparatus, product, or process disclosed, or represents that its use would not infringe privately owned rights. Reference herein to any specific commercial product, process, or service by its trade name, trademark, manufacturer, or otherwise, does not necessarily constitute or imply its endorsement, recommendation, or favoring by the United States Government or any agency thereof, or the Regents of the University of California. The views and opinions of authors expressed herein do not necessarily state or reflect those of the United States Government or any agency thereof or the Regents of the University of California.

The Effect of Precipitated Austenite on the Fracture of a Ferritic Cryogenic Steel

Darrel Richard Frear
M.S. Thesis

Materials Science and Mineral Engineering Department
Lawrence Berkeley Laboratory
Univerisity of California, Berkeley
Berkeley, California 94720

This work was supported by the Office of Basic Energy Science, U.S. Department of Energy under contract number DE-AC03-76SF00098.

THE EFFECT OF PRECIPITATED AUSTENITE ON THE FRACTURE OF FERRITIC CRYOGENIC STEEL

Darrel Richard Frear

Master of Science of Engineering | M.S. Thesis | Physical Metallurgy

Chairman of Committee

ABSTRACT

The effect of precipitated austenite on the fracture of an Fe-8Ni-2Mn-.1Ti steel was investigated. To understand the effect an attempt was made to correlate the microstructure, mechanical properties, and the fracture surface appearance of specimens heat treated to contain austenite or be austenite free. The fracture surfaces were quantitatively studied using a 3D imaging technique in the SEM.

It was found that the presence of austenite had a beneficial influence on mechanical properties by lowering the DBTT. Part of this decrease was found to be due to the austenite gettering deleterious elements off the grain boundaries. Specimens that contained precipitated austenite were also found to have a smaller median facet size, when fractured in a brittle transgranular mode, than specimens with no austenite. The decrease in DBTT and change in fracture surface appearance is related to the austenite transforming to martensite of a different variant than the matrix which effectively grain refines the steel and raises the cleavage stress.

ACKNOWLEDGMENTS

I would like to extend my thanks to the people without whose help this work would have been impossible. First of all I would like to thank my adviser Prof. J. W. Morris Jr. who gave me guidance and support that brought this work to fruition. I would also like to thank the members of the Morris group who made this research a more pleasant experience, and especially Drs. Brent Fultz and Hee Jin Kim and colleagues Young-Ho Kim and Gianni Fior for their enlightening discussions.

My thanks go to the technical staff for their assistance on this project. Jeanne Shull for her careful assistance in preparing this manuscript, Gloria Pelatowski for most of the line drawings, Waylon Wong and the machine shop for the preparation of materials, Harvey Sokol who melted the alloy used in this study, and Ken Gaugler for his assistance on the SAM work.

I would like to thank Prof. R.O. Ritchie and Prof. R. M. Fisher for their review and comments on this thesis.

Last, but definitely not least, I would like to thank my parents for their support in making this whole thing possible.

This work was supported by the Division of Materials Science, Office of Basic Energy Science, U.S. Department of Energy the Materials and Molecular Research Division of Lawrence Berkeley Laboratory under contract number DE-AC03-76SF00098.

TABLE OF CONTENTS

	page
Introduction	1
Historical Review	4
Experimental Procedure	7
Results	
Microstructure	14
Mechanical Properties	20
Fracture Surface Results	23
Discussion	
Microstructure	27
Mechanical Properties	32
Conclusions	41
References	43
Tables	47
Figures	51

INTRODUCTION

There is a need to design a material for use at cryogenic temperatures for both the storage and handling of liquified gases and for fusion energy applications. The basic requirements set for a material to be used for fusion energy are similar to the requirements needed for for storing liquified gases and are as follows [1]:

a) Good strength in small cross section due to the limited space available for the structure.

b) Good fracture toughness.

c) Resistance to low temperature embrittlement.

d) Stable microstructure.

e) Low cost and good domestic availability.

The most widely proposed material for cryogenic structural applications is the austenitic 304 stainless steel series [1]. This material has shown good toughness (200 $MPa(m)^{1/2}$) and somewhat suitable strength (400 MPa) at cryogenic temperatures. Unfortunately 304 stainless steel has disadvantages in that its alloying elements are expensive, there are microstructural stability problems, and there are problems of too much material being needed in cross section for good strength.

Some recent work has been done on high Mn austenitic steel for cryogenic applications [2,3]. In this case the strength has been increased (to 1200 MPa) by hot working the material but the good toughness (230 $MPa(m)^{1/2}$) is retained. However, this steel is still fairly expensive due to the high Cr content. Also working of thick sections of material is not desired due to practicality problems in production.

Due to the considerations of high strength, small sections, and low cost of solute elements work was done to develop a cryogenic ferritic Ni

steel. Ferritic steels have good strength (> 700 MPa) but, unfortunately, they may undergo a catastrophic drop in toughness at a low temperature called the Ductile-to-Brittle Transition Temperature (DBTT), that is common to BCC alloys.

A great deal of research has been done with the goal of dropping the DBTT below service temperature. Some of this research [4,5] has shown that using Ni as a solute lowers the DBTT, and adds to the strength [6]. Research in this laboratory has followed two paths in the attempt to lower the DBTT of ferritic Ni steel. The first line involves refining the grain size of the steel [7-11]. This technique has been able to process a 12Ni steel so that it is ductile down to 4K [12]. The second line of research, and the topic of this thesis, involves the formation of a small amount of precipitated austenite to the ferritic matrix that lowers the DBTT. Several hypotheses have been advanced as to what the function the austenite has on the fracture of ferritic steels. These hypotheses include: 1) The austenite acting as a crack blunter [13-15], 2) the austenite transforming to create regions of residual compression for the volume change of the transformation [16,17], 3) the austenite acting as a sink for deleterious elements [7,18,19] and, finally, 4) the austenite transforming to a variant different than the matrix acting to effectively grain refine the material [20].

The purpose of this research was to investigate the last presented hypothesis of the function of precipitated austenite. By choosing a suitable ferritic steel this hypothesis could be tested be making various heat treatments that would leave the material in states with and without austenite. Then comparing the mechanical properties and fracture surfaces of the specimens the theory can be tested. This research

focuses on how the mechanical properties are affected by the presence of austenite, primarily the toughness at low temperatures. Also the fracture surfaces are analyzed to get a correlation between microstructure and mechanical properties.

HISTORICAL REVIEW

Many beneficial properties have been attributed to the presence of a secondary phase of austenite in a ferritic steel matrix [21-24]. These beneficial properties include an increase in the fracture toughness and a suppression of the DBTT. However, some data [25] shows that the presence of austenite in 12Ni steels is actually detrimental. The work done on 12Ni steel suggested that the austenite formed was not thermally stable and transformed upon quenching to low temperatures. Other work has been done to show that the austenite must be thermally stable to be beneficial [19].

The exact function that precipitated austenite (note that in this work that precipitated austenite refers to austenite that has been formed by tempering in the two phase region, not austenite found upon quenching from the single phase γ region) has on the properties of ferritic steel has been debated for quite some time. Some specific theories have been presented as to how thermally stable precipitated austenite affects the properties of ferritic Ni steels. Some of these theories are presented in the following analysis.

Austenite acting as a crack blunter [13-15]- This hypothesis is based on the assumption that a crack propogating through the steel would be blunted in the ductile FCC austenite, and thus slow crack propogation. This theory was shown to be invalid by Fultz [26], and by Kim and Schwartz [27] who used Mossbauer spectometry and TEM profile microscopy to show that the austenite was mechanically unstable and transformed to martensite in front of the crack and therefore could not blunt the crack.

Austenite transforming to create regions of residual compression from the volume change in transformation [16,17]- This hypothesis has as its basis the mechanism found in TRIP steels where the austenite transforms mechanically in front of the crack. Here the volume change in transformation puts the region in front of the crack into residual compression and thereby slows the crack propogation. However, this transformation results in a small strain which is not believed to be large enough to account for the effects observed. However, this hypothesis is an interesting one and needs further investigation.

Austenite scavenging deleterious elements [7,18,19]- This is a well documented effect. Here the austenite acts as a sink where the deleterious elements, such as S and P, can diffuse in to and thus increase the toughness. Also the precipitated austenite scavenges carbon which lowers the strength but simultaneously raises the toughness.

Crystallographic cleavage impairment model- This hypothesis was first proposed by Morris et al [20]. Before explaining this theory a short digression into the mechanisms of fracture of ferritic steels would be appropriate.

When a ferritic Ni steel is quenched from the single phase γ region it forms a lath type of martensite. The laths tend to bundle together into regions called packets. The laths in a packet are of similar orientation and the variation between laths is at most 2 degrees [28]. Between packets the boundary is generally of a high angle nature [29]. When this steel undergoes brittle fracture cooperative cleavage occurs across the packets breaking across (100) [30], (112) and (123) [31] planes and the crack deviates at the high angle boundary of the packets or the prior austenite grain boundaries. This results in a fracture surface consisting mainly of cleavage facets that correspond well to

packet size [32]. Therefore the effective grain size is in fact the packet size.

When a small amount of austenite (~10%) is precipitated into the martensitic matrix the crystallographic cleavage impairment model comes into play. As stated previously this austenite has to be thermally stable, thermally unstable austenite at best has no effect for it has the tendency to transform to a variant identical to the matrix and would not deviate the crack. However, when the austenite is thermally stable, but still mechanically unstable, it is postulated that in the highly strained region in front of the crack the austenite will transform to a variant of martensite that corresponds to the strain applied. It is probable that this new variant of martensite is different from the matrix [29] creating a high angle boundary. These new boundaries can act to raise the energy needed for fracture to occur making the material tougher. This toughening occurs by making the initiation process more difficult in the same way that making the grain size smaller lowers the DBTT. Therefore by this theory the addition of austenite effectively refines the grain size.

EXPERIMENTAL PROCEDURE

A. Material and Heat Treatment

An alloy of nominal Fe-8Ni-2Mn-0.1Ti was induction melted in an inert Argon gas atmosphere. The alloy was homoginized at 1200°C for 24 hours and then hot rolled into 1/2 inch (12.7 mm) plates. After rolling the material received a heat treatment at 1100°C for 2 hours to anneal out dislocations formed during rolling, followed by an ice water quench. The chemical composition of the alloy is found in Table I.

The heat treatment used in this investigation is based on a modified version of the conventional QLT heat treatment [33], this heat treatment is defined in the Results section. In addition to the QLT treatment three variations were also made Q, QL, and QT. These heat treatments are shown schematically in Fig. 1. The specimens were heat treated in sealed stainless steel bags to reduce high temperature oxidation. The specimens were quenched in an ice water bath at the end of each thermal cycle of the heat treatment. The time at temperature for Q and L was found to be an optimum at 1 hour while the optimum tempering time was 12 hours.

B. Dilatometry

Standard dilatometry specimens (Fig. 2) were machined out of bulk material and were tested, in vacuum, in a Theta Dilatronic III R Dilatometer to determine the phase transformation temperatures (upon heating A_s-austenite start, A_f-austenite finish, upon cooling M_s-martensite

start, M_f-martensite finish). The specimens were heated in an induction furnace with a heating rate of 36°C/second whereupon the specimens were cooled, at a rate of 36°C/second using helium gas as the quenching media, to room temperature.

C. X-Ray Diffraction

X-ray diffraction analysis was done to determine the volume fraction of precipitated austenite formed during heat treatment. Specimens were cut from the bulk material, heat treated, and then mounted in Koldmount. To create a clean smooth surface the specimens were polished by a step-by-step hand grinding an sandpaper, under flood cooling, to 600 grit. To remove any mechanically induced transformation the specimens were chemically etched in a solution containing 5ml HF + 65ml H_2O_2 + 30ml H_2O for 1 to 2 minutes. Once polished these specimens were scanned in a Siemens Kristalloflex X-Ray Diffractometer using $Cu_{K\alpha}$ radiation. The volume fraction of precipitated austenite was calculated using Millers method [34] where the percent precipitated austenite is found by comparing the average integrated intensities of the (220) and (311) martensite peaks to the (211) austenite peak. The formula used was: volume % austenite $=1.4(I_{(211)})/(1.4(I_{(211)} + (I_{(220)} + I_{(311)}/2)$ where the factor of 1.4 is included to take into account the differences of crystallography between the two phases. The samples were rotated between scans to average out the possibility that some preferred grain orientation might have some effect on the true percentage of austenite present. The specimens were quenched into liquid nitrogen for 30 minutes and then scanned in the diffractometer to determine the stability of the austenite.

D. Optical Microscopy

Specimens for optical microscopy were cut form the bulk material, heat treated and mounted in Koldmount. The surface was then ground on sandpaper with flood cooling to 600 grit. The surface was then polished to a mirror finish with 1 micron diamond polishing paste followed by a final polish using 0.3 micron Alumina Oxide. The specimens were etched using a 5% Nital solution and observations were made using a Carl Ziess Metallograph.

E. Transmission Electron Microscopy

The procedure of making thin foils for observation in TEM are as follows. Thin slices of about 15 mil thickness were cut longitudally from broken Charpy specimens using an Isomet diamond wafering blade under flood cooling. These thin slices were then chemically thinned to 5mil thickness using a solution of 5ml HF + 65ml H_2O_2 + 30ml H_2O. Disks of 3mm diameter were carefully punched out using a vise punch to reduce the possibility of creating mechanically induced dislocations. The thin foils were electropolished in a twin jet electropolishing apparatus at room temperature using a solution of 400ml CH_3COOH + 75g Cr_2O_3 + 21ml H_2O. The polishing voltage varied from 20 to 30 volts but polishing current was maintained at a steady 24 mA. Specimens were observed at 100kV in a Phillips EM 301 electron microscope.

F. Scanning Electron Microscopy

The fracture surfaces of broken Charpy specimens were observed using backscattered electrons in the Scanning Electron Microscope. The microscope used was JEOL JSM-U5 Scanning Electron Microscope operated at 20kV. In order to determine the facet size on the brittle fracture surfaces of the Charpy specimens it was necessary to take stereo fractographs tilting the specimen about an axis to image the facets in three dimensions [35]. The SEM used in this study was equiped with a eucentric specimen tilt stage, accurate to ± 0.5 degrees, which simplified this operation. By definition eucentric means that it is possible to tilt and rotate the specimen without the need for changing specimen position of focus because the tilt axis, rotation axis, and optical axis all intersect at one point. The optimal tilt angle was found to be 10 degrees to maximize the features seen in three dimensions. Magnifications were held constant at 500X which was optimal for observing a significant number of clear features of the fracture surface. In order to have a clear unbiased sampling of features on the fracture surface the following procedure was adopted, see Fig. 3. Stereo micrographs were taken at random intervals running across the fracture surface beginning at where the crack initiated, at x=0, and proceeding in the positive x-direction randomly varying the y-direction. An average of 30 pairs of photos were taken per Charpy specimen.

The determination of the inclusions on the fracture surface were done using the Kevex EDAX unit on the AMR-1000 SEM operated at 20 kV.

G. Measurement of Facets in 3-D

Stereo pair photographs of the brittle fracture surface were observed under a WILD ST4 mirror stereoscope. Measurements to determine facet area by the parallax method were made on a CALCOMP 9000 Digitizer. The raw digitized information (containing parallax measurement and perceived facet areas) was sent to an OSBORNE I computer and stored on a floppy disc. Within the computer these data were operated upon sequentially by three programs written by the author. The first program used the parallax measurements to compute the true facet area of the facets, the second program put these facet areas in an increasing sequential order so that the third program would create a histogram to show the distribution of the data. A flow chart of this process is found in Fig. 4.

H. Theory of 3D Stereo Fractography

Stereo microscopy is of great use in observing fracture surfaces and making quantitative analyses [36]. Stereo microscopy is a method by which one is able to gather the true information off the fracture surface, not the perceived two dimensional information.

A schematic drawing of the process of photographing a three dimensional micrograph is seen in Fig 5, and the following equations follow the symbolism of this figure.

Z_c = Difference in height in central plane of feature

P = Parallax value

α = Half the total tilt angle from the left plane projection to the right plane projection

so:

$$Z_c = D_r - D_l / 2\sin(\alpha) = P/2\sin(\alpha)$$

now:

θ= The angle between the feature and its normal

so:

$$\tan(\theta) = Z_c / A_{1'} C_{1'}$$

$$\theta = \tan^{-1}(Z_c / A_{1'} C_{1'})$$

True Area = True area of feature

Inclined Area = Apparent area as measured off the left plane projection (measured in 2D)

therefore:

True Area = (Inclined Area)/cos(θ)

To get the true area of the facet the magnification M must be taken into account. The above equations give the area of the feature in the magnified micrograph as measured by the digitizer. Therefore the final result is:

Area of Feature = True Area/M.

I. Charpy Impact Testing

After heat treatment standard V-notch Charpy specimens were machined and made to a ground finish, Fig. 6. One set of Charpy specimens were tested with the V-notch, a second set were tested after a sharp fatigue crack was formed starting at the V-notch and extending 1mm into the specimen. The specimens were tested using a Charpy Impact test machine with a 60 lb (27.3 kg) hammer to determine the DBTT curves. For temperatures ranging between liquid nitrogen and room temperature a bath

mixture of liquid nitrogen and isopentane was made. For liquid helium testing the styrofoam box method proposed by Kim [37] was used, Fig. 7.

J. Tensile Testing

Tensile tests were performed using subsized flat tensile specimens, Fig. 8,machined from heat treated blanks. Testing was performed on an Instron model 1332 testing machine at a strain rate of $5x10^{-4}$ in/sec ($1.3x10^{-3}$ cm/sec). Specimens were pulled at room temperature, liquid nitrogen (77K) temperature, and at intermediate temperatures. From temperatures between 77K and room temperature a mixture of liquid nitrogen and isopentane was used in a suitable cryostat. The yield strength was calculated using the 0.2% offset method. Both total elongation and the percent reduction in area were determined using a traveling light microscope accurate to $\pm$0.01mm, with the total elongation determined by measuring the difference between scribe marks on the gauge length before and after testing.

RESULTS

Microstructure

The material chosen to do this study was an 8Ni-2Mn-0.1Ti steel with the full composition found in Table I. This composition was chosen for a number of reasons. The Ni was added because of its known good cryogenic properties, and this study was made to be applicable to Ni steels. The Mn was added because it is known to be an austenite stabilizer [38,39] and from previous research [19] it has been seen that the austenite necessarily has to be thermally stable. The small amount of Ti was added to getter carbon. A low C content was desired because the carbon tends to form carbides upon heat treatment and these carbides add a complicating factor to both the microstructure and the mechanical properties [7] that could confuse the effect that austenite has on the steel. Finally this alloy was also chosen because some previous research on a similar alloy [40] inferred that the presence of austenite alone had the effect of lowering the DBTT.

To determine the heat treatment the transformation temperatures were found by dilatometry. Fig. 9 shows these results plotted and includes the austenite and martensite start and finish temperatures. Based on these results an approximate phase diagram can be drawn, Fig. 9, from which a heat treatment can be designed.

Portions of the QLT heat treatment [33] were chosen to observe the effect of the precipitated austenite. The treatments will be called Q, QL, QT, and QLT and each treatment is described below and can be seen schematically in Fig. 1. The Q and QL treatments are control specimens,

they do not contain austenite. Q and QL are to be compared with the QT and QLT treatments that do contain precipitated austenite. The Q treatment is just into the single phase austenite region at 750°C for 1 hour, and like all treatments is followed by an ice water quench. The L treatment is an intercritical anneal at 660°C for 1 hour. The T treatment is an intercritical tempering treatment at 550°C, above the temper embrittlement region [41,42] of this alloy, designed to precipitate stable austenite because of the higher solute content at this lower temperature. To determine the tempering time QLT and QT specimens were tempered for various times and were analyzed by x-ray diffraction to get the volume percent of austenite present. These results are plotted in Fig. 10 as a function of tempering time. The volume percent of austenite increases, in a somewhat linear fashion that seems to level out after 10 hours, from 0% for both QT and QLT (there is no austenite in Q or QL) to a value of 6% for QT and 10% for QLT. As can be seen the 12 hour temper results in a suitable amount of austenite in both QT and QLT for originally about 10% austenite was desired. The thermal stability of this austenite was checked by quenching the specimens down to 77K and this is also plotted in Fig. 10. It can be seen that this austenite is stable losing little or no austenite upon quenching.

Optical Microstructure

The microstructure as observed through the optical microscope is shown in Fig. 11 for each heat treatment. This structure of irregular boundaries is common to low carbon Ni steels [12,40,43]. The micrographs show very irregular boundaries that become more defined into a substructure in the QT and QLT specimens. No obvious prior austenite grain boundaries could be observed. The average size of these bounded

regions (for QT and QLT) was measured to be about 500 μm^2. Observation of these boundaries in SEM showed that the Nital etch had preferentially attacked these regions. Other than the above little information of the microstructure could be garnered from the optical microscopy study. The Transmission Electron Microscope (TEM) was then used to determine the the microstructure of this alloy and its heat treatments.

TEM Microstructure

Using TEM it was possible to determine the microstructure of this 8Ni-2Mn steel. Each heat treatment resulted in a different microstructure that affected the material properties.

Q microstructure- Fig. 12 shows the typical highly dislocated lath microstructure found in the Q condition. Here the material has been quenched from the single phase region and has undergone a martensitic phase transformation. There is no retained austenite present and the lath structure results in a single diffraction pattern. This is in accord with the results of Morris et al [20], Wayman [28], and Naylor [29] who state that laths are misoriented by a maximum of a few degrees and that the laths are similarly oriented in the same packet. The average lath width is approximately 0.4μm and the laths are more or less parallel to the (110) plane. It is difficult to get a good clear image of the microstructure due to the large number of dislocations present. Figure 13 is another micrograph that shows the highly dislocated structure and here the (110) lath plane is shown along with the (100) cleavage plane showing that transgranular fracture is also trans-lath.

Figure 14 presents an interesting view of the Q condition near to what is believed to be a packet boundary. The diffraction pattern in taken from the region bounded by the arrows and the [023] pattern be-

longs to the region in the upper right hand corner of the micrograph, while the [001] pattern corresponds to the structure in the left hand side. It is interesting to note that the region in the upper right hand portion consists of laths running perpendicular to the paper while the rest of the laths are parallel to the page. This is direct evidence that the microstructure consists of rod like laths and not plate martensite. Notice also that the boundary separating the two regions has a smooth curvature. This could imply that it is a prior austenite grain boundary but the region bounded is rather small, as seen in the microscope, so it could be that the boundary is a packet boundary. This is in contrast with work done by Kim [44] who found that packet boundaries are very irregular in a rapidly heat cycled specimen. However, these irregular boundaries seem to be found only in rapidly heat cycled specimens, not as quenched steel, and could explain the good properties found in the heat affected zone in welded 12Ni steel.

QL microstructure- Fig. 15 is an example of the typical microstructure of this heat treatment. For the QL treatment the material was intercritically annealed for 1 hour and then quenched to $0^{\circ}C$. During intercritical annealing steel has both α and γ present but upon quenching the γ is solute lean so it is therefore thermally unstable and transforms to highly dislocated martensite. No austenite is expected to be present in this microstructure and this can be seen in the diffraction patterns of the QL condition where a clean single pattern is present, and an x-ray study confirmed the matrix to be austenite free.

In Fig. 15 it can be seen that the microstructure has been changed a great deal by the L treatment. The matrix has undergone polygonization and recovery, the lath structure has been eliminated and polygonized subgrains result. These polygonized subgrains have a low angle

boundary between them but the packet boundaries still remain high angle. Also notice that the matrix has had many of the dislocations annealed out and the microstructure is "cleaner", and a sharper image results as compared to the Q condition.

The dark fuzzy regions in the center of Fig. 15 are believed to be austenite that has thermally transformed to martensite upon quenching. The "fuzziness" is due to the high density of dislocation present in the particles of fresh martensite. These particles have also transformed to a variant identical to that of the matrix. Also note that in the matrix near these transformed particles there is a network of dislocations running out of the particles. These networks are thought to be due to the strain imparted into the matrix when the austenite transforms from the close-packed FCC phase to the BCC phase. Fultz, et al. [45] have done an interesting study of this transformed austenite in overtempered 9Ni steel and found it to have a deleterious influence on the material properties.

Figure 16 is another micrograph of the QL condition and here it can be seen that the transformed particles (in the top portion of the micrograph) still seem to be along the {110} planes. Again it can be seen in this photo that the microstructure is polygonized and has gone through a recovery process.

QT microstructure- Figures 17-20 are typical examples of the QT microstructure, bright field and dark field pairs of austenite taken from the $(200)_\gamma$ spot. In this heat treatment the material is intercritically tempered and the austenite has had a chance to become solute rich and therefore thermally stable, and this results in 6% austenite.

In Fig. 17 it can be seen that the matrix has polygonized and

undergone recovery but not to the same degree as in the QL condition. This can also be seen in Fig. 18. The matrix still appears to contain quite a few dislocations, but a great number have moved to subgrain boundaries resulting in the same kind of polygonized structure seen in the QL microstructure.

The austenite that has formed in Figures 17-18 also lies along {110} planes and is found to be in the Kurdjomov-Sachs [46] (K-S) orientation relationship, although the Nishiyama-Wasserman [47] (N-W) relationship was observed though not photographed. The austenite has a long elongated morphology and has an approximate 1μm x 0.15μm dimension. Fig. 19 shows that this some morphology but here the austenite is not parallel to the page but at some angle out of the page.

Figure 20 shows an interesting QT microstructure. Here the lath structure has been maintained with some precipitated austenite falling between the laths on the (110) planes, in a K-S orientation relationship. Note that the microstructure is still heavily dislocated. A possible reason why the matrix has not polygonized in this case is presented in the Discussion.

QLT microstructure- Typical examples of the QLT microstructure are found in Figures 21-23. This heat treatment takes the QL microstructure and adds an intercritical temper that creates 10% austenite. The austenite can form easily because of the slightly solute rich regions left from the austenite that formed and transformed on quenching during the L treatment.

The matrix of the QLT heat treated specimens is very much recovered and has undergone polygonization. Very few dislocations are left as can be seen in Fig. 21. Here the matrix is clean enough to see remaining single dislocations (found in the lower right hand side of the micro-

graph). In the left center portion of Fig. 21 a good example of polygonization can be seen where the dislocations have aligned themselves into parallel lines. This effect can also be seen in Fig. 22.

The austenite present presents both the N-W, Fig. 21, and the K-S, Fig. 22, orientation relationships and the austenite still lies along (110) planes. The morphology of the austenite present appears to be elongated and perhaps a bit thicker than found in the QT condition with dimensions of approximately 1.5μm x 0.2μm. The larger size of austenite is probably due to the double tempering allowing the austenite to nucleate faster because there are solute regions remaining from the L treatment allowing more time during the tempering for growth.

Another interesting feature is found in the austenite particle found in the lower right hand corner of Fig. 23. In the dark field a cross hatch of dislocations can be seen running across the particle. This is thought to be due to the misfit between the BCC and FCC phases creating dislocations at the interface to take care of this crystallographic misfit. The dark parallel lines running around the austenite particles, in bright field, are wedge thickness fringes.

Mechanical Properties

Charpy impact tests were performed to determine the ductile-to-brittle transition temperatures for the various heat treatments using ASTM standard V-notch specimens. The results of these tests are plotted in Fig. 24. The first notable point is that the upper shelf energies are all similar so the addition of austenite did not confuse the results of DBTT shift with an upper shelf change as seen by Kim [7]. The DBTT of the austenite containing samples (QT and QLT) are the lowest, the shifts in transition temperatures and the transition temperatures

themselves are found in Table II. In this work the definition of the DBTT is taken as being that temperature for the given energy that is midway between the upper and lower shelf energies. The lower shelf energies for both QT and QLT are slightly raised above Q and QL. However, the lower shelf energies are very small, on the order of a few foot-pounds (or J), so any small increase in energy is actually a large percentage increase. Therefore the results of lower shelf energies are in the region of large experimental error.

The high DBTT of the Q condition is due to the fracture being intergranular which drastically affects toughness. This feature will be discussed later.

To confirm the results of the first test a second set of Charpy specimens were tested. This test was performed using the fatigue pre-crack Charpy specimen, with a sharp crack 2mm long at the root of the V-notch. These results are plotted in Fig. 25. This test does confirm the previous results and these transition temperatures and shifts in transition temperatures along with the shelf energies are found in Table II. Again the Q samples fractured intergranularly and the specimens containing austenite showed the lowest DBTT and the highest lower shelf energy. There appears to be a significant difference between the fatigue pre-crack sample and the blunt notch in the impact energies and the shape of the curves. The presence of the sharp crack lowers the impact energy by half, which is to be expected for the presence of the crack eliminates 25% of the volume of material the crack has to propogate through. The shape of the transition curve is also affected be the presence of a sharp crack.

The above results indicate that the austenite does have an affect

on the DBTT of this material similar to the effect as seen be Jin, et al. [40]. However, the Charpy impact test by itself cannot be used by itself as proof that the austenite is the sole cause of the shifts in DBTT, in fact the results seem to show that the austenite is having a much larger effect than is to be expected. Therefore other mechanical properties must be found as well as a microscopic study of the fracture surface must be performed.

Tensile Test Results

Tensile tests were performed on flat tensile specimens at various temperatures between 77K and room temperature. These results are tabulated in Table III. Specimens heat treated in the Q condition were tested at only 77K and room temperature because Charpy data, and later fracture surface observations, indicated that this heat treatment resulted in intergranular fracture and thus extensive tensile data were deemed unimportant. However, the specimens tested in the Q condition showed the highest yield strength which is expected because of the large dislocation density in the as quenched condition.

The yield strength verses temperature is shown plotted in Fig. 26. As can be seen the QT heat treatment has the highest yield strength for all temperatures, followed by QL, with QLT having the lowest yield. This can be explained, at least qualitatively, if a dislocation density argument is used. There are more dislocations present in the QT microstructure, as seen in TEM, and the higher the density of dislocations the larger the yield stress. Likewise the QLT microstructure has recovered many of its dislocations and has a lower yield strength. This point will be covered in more depth in the Discussion.

An engineering stress-strain diagram is shown in Fig. 27 for the

four heat treatments tested at 77K. The trends seen in these curves are applicable to the higher temperature tests. The first noticeable feature is the yield point seen in the QT treatment. This is interesting because there is a very low interstitial content in this alloy so dislocation pinning by interstitial atmospheres is unlikely. However, a possible explanation is that the high dislocation structure still present in the QT condition is being pinned by the dislocated polygonized structure itself [48] or the precipitated austenite is somehow pinning the dislocations up to yielding for the austenite transforms to heavily dislocated martensite upon straining and these fresh dislocations may act as a barrier to dislocation flow.

Another interesting trend seen in the yield data concerns the percent total elongation. The elongation and the percent reduction in area is seen to increase from Q to QL to QLT the most elongation in QLT. This may be explained by the presence of the austenite giving the material a "dual-phase" property. The austenite transforms past the yield point adding to the total elongation, so the austenite gives some added plasticity to the matrix during yielding. Also it is seen that the elongation and percent reduction in area increase with decreasing temperature for all the heat treatments.

Fracture Surface Results

Quantitative results were obtained from the fracture surfaces of the broken Charpy specimens. There are three possible fracture surfaces that can be observed. The upper shelf fracture surface, the fracture surface of the transition region, and the lower shelf fracture surface.

The upper shelf fracture surface consists of 100% ductile dimples, an example of which can be seen in Fig. 28. The upper shelf fracture

surfaces of all four heat treatments were identical. The inclusions seen in Fig. 28 were analyzed using EDAX in the SEM and were determined to be MnS.

The appearance of the fracture surfaces of the transition region is termed quasi-cleavage, part brittle fracture and part ductile fracture. These fracture surfaces were not investigated in this study. A study done by Fior [36] of 6Ni steel quantitatively analyzed the fracture surfaces of this region.

For this study the brittle fracture surfaces were quantitatively analyzed for each of the various heat treatments. Fig. 29 shows typical fracture surfaces of the four heat treatments. In the Q condition there has been an intrusion of intergranular fracture, as pointed out by the arrows in Fig. 29A. This accounts for the high DBTT in the Q condition. A Scanning Auger Microscopic analysis of the fracture surface is seen in Fig. 30. To do this analysis a specimen was broken in situ at 77K and the Auger analysis was taken from an intergranular region. From this analysis it was determined that there is 60x the amount of P present at the intergranular regions as is present in the bulk. Phosphorus must then segregate to the prior austenite grain boundaries during the austenitizing treatment and cause intergranular fracture as is well documented [49-52]. Despite this intergranular fracture there appear to be large facets present. Unfortunately, these cannot be measured quantitatively because of the intrusion of intergranular fracture. The other three treatments can be measured quantitatively for the fracture surface in each contains solely transgranular fracture. In the two dimensional micrographs of Fig. 29 the fracture surfaces of QT and QLT appear to be more broken up than in the QL condition.

To be able to get the true facet size a three dimensional technique was used, as is detailed in the Experimental Procedure. For this work it is necessary to have a definition of what a facet is to keep the measurements objective. A facet is here defined as being a flat region, on a brittle fracture surface, that has some kind of river patterns running across it. Some typical facets are outlined by the arrows in Fig. 31. To get good statistics approximately 1000 facets were measured for each heat treatment using four broken Charpy specimens per heat treatment.

The results of this quantitative study are presented in the histograms of Fig. 32. It can be seen that by comparing the three histograms that QL has an even distribution of facet areas while QT and QLT have the majority of facets at the lower end of facet areas. The median values for each heat treatment are: QL = 560μm^2, QT = 225 μm^2, QLT = 219 μm^2. The median value is used because it is not influenced by an anomalous large or small number as the mean value can be.

From this result it is apparent that the presence of austenite does in fact create a smaller facet size. However, all three heat treatments do have some large facets so the austenite does not refine all the facets. The fracture surfaces of QT and QLT are similar with QLT having a slightly larger number of small facets present. This small difference could be due to there being a larger percentage of austenite present in QLT, manifested in the slightly larger austenite particle size, possibly creating a more defined high angle boundary. Also the difference is so small it could very well be explained as being experimental error. It is also interesting to note that in QT and QLT there are a smaller number of large facets (facets of area greater than 900 μm^2) present than in QL. This appears to be a true result and not a function due to

error in sampling. It was observed that the angle of deflection of the crack observed from profile fracture surfaces was around 45° for both specimens with and without austenite.

DISCUSSION

Microstructure

In order to understand the effect that precipitated austenite has on the toughness, and the mechanics of fracture, of this 8Ni-2Mn steel the microstructure must be fully examined. For this examination the four heat treatments Q, QL, QT, QLT were tested and were found to have differences, both subtle and dramatic. Some work done by Kim, et al. [53] discusses how the QLT heat treatment works in a 6Ni carbon containing steel and what the microstructural changes are. There are some definite similarities between the 6Ni case and the present 8Ni-2Mn steel used in this study. In the following these differences will be discussed, along with a discussion of the formation of the austenite itself.

The as-quenched (Q) microstructure shows that the transformation from the single phase γ region to room temperature results in a highly dislocated lath type of martensitic microstructure, Fig. 12, with no retained austenite found in the matrix upon quenching. The crystal structure found here is not the typical BCT found in carbon containing martensitic steels because the carbon content of this 8Ni-2Mn steel is very low. Therefore it is not possible for the carbon to cause a tetragonal distortion. The Q microstructure is heavily dislocated due to the strain involved in transforming from the close packed FCC to the more open BCC crystal lattice. The matrix takes up this strain in the form of dislocations. The Q treatment also has use as a grain refinement treatment [7]. This effect was not investigated in this study and all heat treatments began with just one Q treatment. Therefore for all heat treatments the grain size was constant and did not act as a further

variable to the research.

There is little to no chemical segregation during a martensitic transformation and this is detrimental to the properties of the Q heat treatment. During the single phase treatment P segregated to the austenite grain boundaries and stayed there during the martensite phase transformation. It is well known [49-52] that P being present on grain boundaries tends to cause intergranular fracture, and this occurred in this steel, Fig. 29, which shows approximately 40% intergranular fracture. The intergranular fracture also raises the DBTT to near room temperature, Figures 24-25. The Auger analysis showed that 60x the amount of P was present at intergranular regions as found in the bulk, see Fig. 30. This would seem to indicate that P segregation was in fact the cause of the intergranular fracture.

The other three heat treatments QL, QT, QLT involve two phase tempering during which some austenite is formed. The thermally unstable austenite formed in the QL treatment will be discussed later, but the following concerns the formation of thermally stable austenite formed during the 550°C temper.

When austenite forms in a BCC matrix it tends to form on the {110} planes in a K-S [46] orientation relationship: $(110)_{bcc}//(111)_{fcc}$, $[1\bar{1}1]_{bcc}//[0\bar{1}1]_{fcc}$ or the N-W [47] orientation relationship: $(110)_{bcc}//(111)_{fcc}$, $[001]_{bcc}//[\bar{1}01]_{fcc}$. Both of these orientation relationships were observed, see Figures 21-22. There are two reasons why the $(110)_{bcc}$ plane is selected by the austenite: 1)This plane offers the least misfit between the BCC and FCC phases so the least strain energy is created by forming austenite on this plane, 2)martensite laths tend to lie along (110) so the austenite will lower the energy of the lattice

if it forms to destroy a boundary. However, austenite is not likely to be found on packet or grain boundaries even though the energy of the crystal would be lowered, because it is probable that one side of the austenite could have a K-S or N-W relationship but the other side would lie in a region of a different crystallography, this would put half of the austenite particle is a state of high strain energy.

The austenite formed at 550°C will be solute rich following from the lever rule applied to the phase diagram of Fig. 1. This stabilizes the austenite down to room temperature and even down to 77K, Fig. 10. A previous STEM EDAX study [7] of precipitated austenite showed solute enrichment in austenite of a 6Ni steel. A STEM EDAX analysis of this 8Ni-2Mn steel also showed solute enrichment in the austenite with the results shown in Table IV. From Table IV it is clear that there is a strong Ni and Mn enrichment in the austenite with Fe being depleted. Overtempering to form a large fraction of precipitated austenite has been seen to have a deleterious effect on material properties [7,45]. The reason for this is that during long time tempering the solute content of the austenite does not increase but in fact decreases as averaged over the volume of the austenite. This tends to make the austenite thermally unstable. Overtempering was not a problem encountered in the QT and QLT specimens for the austenite that was formed here was found to be thermally stable.

During the 550°C temper the formation of austenite is not the only microstructural change that occurs in the matrix, the dislocation structure is also altered. When tempered the highly dislocated martensite undergoes recovery and polygonization. Recovery is the process of annealing out dislocations to grain boundaries or the simple annihilation of the dislocations (this can be thought of as bringing two edge

dislocations of opposite sign together). Polygonization is the movement of dislocations to form low angle boundaries, that lower the energy of the crystal, by glide and climb. The result of these two dislocation processes is that the lath structure is lost to polygonized sub-grains and within these sub-grains the matrix has been "cleaned" of dislocations by the recovery process. This type of structure is seen in all two phase tempered specimens QL, QT, and QLT. QLT, the double tempered specimen, of course has the most dislocation free matrix, as seen in Fig. 21, because it has been tempered longer with both an intercritical anneal and temper.

A very interesting point concerns the dislocation density difference between QT (12 hours at 550°C) and QL (1 hour at 660°C). Qualitatively, from TEM micrographs, it is seen that QL has fewer dislocations than QT. This is confirmed by the yield data of Fig. 26 that show QT has a higher yield strength than does QL. A material undergoes yielding at the onset of plastic deformation. It is difficult for a material to yield when a large number of dislocations are present keeping the material from flowing plastically. Q would then, of course, have the highest yield strength, and in fact it does. The question then to be asked is , why is the dislocation density lower in QL than QT? This can be explained using a diffusion argument. As a first approximation dislocation climb can be thought of as Fe self diffusion (as climb would be the rate limiting step in dislocation motion). Fig. 33 shows a plot of the log of diffusivity (in cm^2/second) versus 1/T for Fe self diffusion [54]. Using the solution to the diffusion equation $x=(2Dt)^{1/2}$ where x=distance travelled, D=diffusivity, and t=time. By using Fig. 33 it is found that: $x=2x10^{-6}$ cm^2/s for L(1 hour at 660°C) and $x=8x10^{-7}$

cm^2/s for T(12 hours at 550°C). Therefore in one hour at 660°C dislocations should be able to move farther than in 12 hours at 550°C. This could explain the difference in dislocation density and the difference in yield strengths for the QL and QT heat treatments.

In Fig. 20 of the QT treatment a lath structure can still be seen sandwiched between austenite particles. This is the result of the austenite forming at the lath boundaries before polygonization has a chance to take place. The austenite acts to hold the dislocation structure in place. Evidence that austenite does form before polygonization can be seen from Fig. 33 where the diffusivities for Fe self diffusion, Ni in Fe diffusion [55], and Mn in Fe diffusion [56] are shown plotted versus temperature. It can be seen that at 550°C Mn and Ni are able to diffuse faster than Fe self diffusion (which is approximated as the dislocation "diffusivity", or the rate at which recovery and polygonization can occur) so the austenite would be able to form before polygonization. This also shows why Mn is such a good austenite stabilizer [38,39], it is able to diffuse to the austenite very quickly and make the austenite solute rich.

The QL microstructure is also interesting and follows from the above discussions. During this treatment austenite does form although it is solute poor and transforms to heavily dislocated martensite upon quenching to room temperature, Fig 15. This fresh martensite is slightly solute rich (which in the QLT heat treatment assists in the formation of stable austenite on tempering at 550°C) and has the same crystallographic orientation as the matrix. This can be explained using the K-S and N-W orientation relationships. When the austenite forms on heating it will take the most energetically favorable orientation, some variant of K-S or N-W, and upon quenching it will transform back to the variant

it came from, and this variant should be the one that is still the most energetically favorable.

The QLT microstructure is a combination of QL and QT. During the L treatment the matrix polygonizes and forms slightly solute rich regions. During the T treatment the austenite has a chance to form with stability and recovery occurs to a great extent, as seen in Figures 21-23. This extensive recovery also explains why QLT has a low yield strength. More austenite forms during QLT than QT because the austenite is slightly larger in QLT for solute diffusion occurs readily during the double temper, and this results in the 4% difference of γ content between the two heat treatments.

Mechanical Properties

The presence of precipitated austenite in a ferritic matrix has been seen to have a beneficial influence on the mechanical properties of those materials tested [21-24,40]. The work done here on 8Ni-2Mn steel shows that the precipitated austenite is beneficial for cryogenic mechanical properties. The intent of this work was to gain some understanding of how the austenite does influence the properties. Unfortunately the effect is not simple and clear cut, the many variables present in heat treating steel also have effects on the material properties. However, it is possible to sort through these varied effects and make some statements about how the austenite affects this cryogenic steel.

From Fig. 26 it can be seen that by varying the heat treatment the yield strength of the steel also varies.

The differences in yield strengths may be explained if thought is given to what the dislocations do during heat treatment. An increase in

the density of dislocations in the bulk of a material results in an increase in the yield strength, it takes more force to move a great number of dislocations through a material than a few and this large number of dislocations may tangle and pile up adding to the force needed to yield. This is stated formally in the following equation:

where: $\sigma = \sigma_0 + k\rho^{1/2}$

σ_0, k are constants

σ = applied stress

ρ = dislocation density

Thus the stress varies with the square root of the dislocation density. In the Q condition the matrix is a highly dislocated microstructure of lath martensite. When the material is tempered high in the two phase region, the L treatment, many of these dislocations anneal out to the boundaries, both packet and polygonized grain boundaries. But at the same time some dislocations are imparted to the matrix from the transformation of the thermally unstable austenite, but these few dislocations are localized and not enough are formed to drastically change the dislocation density. When the material is intercritically tempered for 12 hours, QT treatment, a different dislocation density results. Here the dislocations are not able to move as quickly to the boundaries (as stated previously in the Microstructure Discussion) so even after 12 hours the dislocation density does not decrease as much as it does after one hour in the L treatment. In the QLT condition the yield strength is lower than both QT and QL and this can be explained using the above arguments. The L treatment anneals out many dislocations and the tempering treatment, T, anneals even more out to lower the yield strength further.

The effect that austenite has on fracture toughness can be seen in

the DBT curves of Figures 24-25. The curve for the Q treatment is left from discussion due to the intrusion of intergranular fracture. However, it can be seen that the austenite containing heat treatments QLT and QT have a lower DBTT than QL which has no austenite. The presence of austenite lowering the DBTT has been seen in other work [7,40].

Unfortunately the effect of the presence of precipitated austenite is not clear from the DBT curves because the yield strength varies. As can be seen in Fig. 34 the DBTT can be lowered by decreasing the yield strength. However, between the QL and QT heat treatments QT has a higher yield but a lower DBTT. The DBTT of QT is only 5-10°C below that of QL but this is significant due to the higher yield strength of QT, if the yield strengths were equal there would be a more noticeable drop in DBTT.

The reason that QT and QLT have a lower DBTT than QL is due to the austenite acting to raise the critical cleavage stress of the material, as seen in the schematic diagram of Fig 34. Indirect evidence that the cleavage stress has in fact been raised can be gathered from the tensile fracture stress and lower shelf energies of the Charpy specimens. The cleavage stress is that stress, at a low temperature, at which a material will fracture in a brittle fashion. The addition of austenite raises the lower shelf energy (Table II, note that QT and QLT have larger lower shelf energies than QL), and the fracture stress is larger for QT and QLT that QL at temperatures below the DBTT (Table III) where cleavage stress comes into play. These measurements are not the best to determine cleavage stress, fracture stress measurements in 4 point bending would be much better (and for a more complete analysis should be performed), but they can be used as a good indication. The significance

of Fig. 34 is that at a given temperature the material will break in a ductile or brittle fashion depending upon whether the isothermal line intersects the yield stress curve or the cleavage stress curve first. The yield stress is known to vary with temperature but the cleavage stress is assumed to be relatively independant of temperature. Where the cleavage stress curve intersects the yield stress curve can be called the DBTT. It can be seen that by raising the cleavage stress that the DBTT will drop. In Fig. 34 σ_c refers to the cleavage stress and $\sigma_{c+\gamma}$ refers to the cleavage stress due to the presence of austenite. By raising the cleavage stress it can be seen, qualitatively, how it is possible for QT to have a lower DBTT than QL even though it has a higher yield strength. Measuring the cleavage stress in a quantitative form is difficult due to the inseperability of cleavage stress and yield stress. This makes Fig. 34 purely qualitative, but even from this simple diagram it is possible to gain some insight into how even though the yield stress varies the DBTT may drop.

The raise in cleavage stress can also be reflected in the lower shelf energies of Figures 24-25. The heat treatments QT and QLT have larger lower shelf energies than QL but as discussed earlier a small difference at this low energy value appears to have large absolute affect. Therefore it is possible that experimental error could have a large influence in the lower shelf energy. If QT and QLT have a similar cleavage stress they should also have the same lower shelf energy, but QLT has a higher lower shelf energy. This could be due to the above error discussion, or the difference could be due to the QLT lower shelf energy given does not lie on the same position of the tail of the curve as does QL.

It has been seen that precipitated austenite does affect the frac-

ture process but it is still unclear as to exactly what the austenite does during fracture. Three viable hypothesis have been proposed as to how austenite influences fracture. Each of these hypotheses will be discussed in turn.

Austenite acting to getter deleterious impurities [7,18,19]- This is a well documented effect and was seen to have an effect in this study. The intergranular fracture of the Q specimen was found to be due to the presence of a large quantity of P at prior austenite grain boundaries. After an intercritical temper and the formation of austenite, thermally stable or unstable, it is thought that the P segregated off the prior austenite grain boundaries and into the austenite. The cleavage stress for intergranular fracture is much lower than that of transgranular fracture. By eliminating intergranular fracture the low transgranular fracture stress was eliminated, as well, and the DBTT drops dramatically for intercritically tempered materials.

Crystallographic cleavage impairment model [20]- Basically this theory involves the austenite in front of the crack transforming to a variant of martensite that is different from the matrix, and effectively grain refines the material. The presence of additional high angle boundaries makes the initiation and propogation of cracks in the material more difficult due to larger numbers of cleavage cracks that must form for the main crack front to advance. This toughens the material by raising the stress needed for cleavage cracking to occur, and is similar to grain refining the material. The resulting crack path from the above hypothesis is shown schematically in Fig. 35. The idea that the transformed austenite would create a high angle boundary was proposed by Morris et al [20] and has been discussed by Naylor [29] who went through

the possible number of variants available from the K-S orientation relationship and found that there is a good probability that a high angle boundary will form.

In a martensitic material that does not contain austenite the crack is deflected or reinitiated only by the high angle boundaries present from prior austenite grain boundaries and by packet boundaries. The result of this is that the brittle fracture surface of material with no precipitated austenite will have facets that correspond to the packet size [31]. This can be seen to be indirectly true from the present study. The median cleavage facet size from the QL specimens, with no austenite, is approximately the same size as what are believed to be packets from the optical microstructure, Fig. 32.

If the crystallographic cleavage impairment model is indeed valid the brittle fracture surface appearance of specimens containing a significant fraction of precipitated austenite should be broken up and the median facet size should be significantly smaller. The median facet size was in fact seen to decrease in the QT and QLT specimens and the fracture surfaces of both heat treatments were similar. This similarity could be due to both heat treatments containing a significant fraction of precipitated austenite. The angle of deflection of the crack at high angle boundaries has been seen to increase the toughness of a material if the angle is large [57]. However, this mechanism was not observed in the brittle fracture surfaces of this study because the angles of deflection were similar for both specimens with and without austenite. The fact that there are more large cleavage facets in the QL condition than in the QT and QLT specimens is also significant. This could be as important as the shift in median facet size. This could imply that the austenite toughens the material by breaking up the large packets fol-

lowing the crystallographic cleavage impairment model. That is to say that the presence of large facets on a fracture surface implies poor toughness, so when these large facets are broken up into finer facets the material is toughened. It is interesting to note that even though there is a 4% difference in the amount of precipitated austenite between QT and QLT the specimens revealed brittle fracture surfaces that are similar. This could be the result of the austenite forming in similar regions of the microstructure for both heat treatments. For both QT and QLT the austenite is found to form along (110) and it is possible the only difference in the volume percent of austenite is the size of the particles, the distribution is similar. This would indicate that it is not the size of the austenite particles but that there is a distribution of austenite particles that transform, in front of the crack, to create high angle boundaries. A future experiment involves testing this idea by tempering 8Ni-2Mn steel for a short time to develop austenite that has a fine distribution, but small size, to see if even is this case the brittle fracture surfaces show refinement.

The exact procedure by which dispersed regions of rod-like transformed austenite grain refines the steel is somewhat difficult to understand but the following may add some light to the subject. The crack propagates across a single cleavage plane as it traverses a packet and will only be reinitiated or deflected if the transformed austenite is oriented correctly, namely the long axis of the austenite in the same plane as the crack. Austenite forms on (110) and cracks tend to propogate along (100) (see Fig. 13), and this will tend to put the crack and austenite in a good orientation. What will also help to allow the austenite to form a continuous high angle boundary is that the austenite

is fairly continuous along (110), Fig. 36, and that this austenite will all transform to a similar variant that is different form that within the packet, which is reasonable as the strain field in front of the crack within the packet should be constant. The transformed austenite acting to create high angle boundaries and effectively grain refine the steel is certainly not a simple mechanism, in fact the process is most certainly a very complicated one and is worthy of further study.

Austenite transforming to create regions of residual compression[16,17]- This hypothesis was not studied in this work but is worthy of some discussion. In this theory the act of transforming the austenite in front of the crack creates regions of residual compression due to the volume change in transformation that acts to toughen the material. This is a plausible theory but the effect is deemed to be small for there is only a 4% change in strain going form austenite to martensite. Using the formulation provided in McMeeking and Evans [58] for a second phase transforming in front fo a crack in a brittle material an estimate as to the magnitude of this effect may be calculated. By performing this calculation for the upper limit case (the largest plastic zone size etc.) it is found for a material containing austenite with a fracture toughness (by 3-pt. bend test) of about 100 ksi(in)$^{1/2}$ (689 MPa(m)$^{1/2}$). Without austenite present the toughness is about 80 ksi(in)$^{1/2}$ (550 MPa(m)$^{1/2}$). The change in toughness due to the austenite transforming adds 11 ksi(in)$^{1/2}$ (77 MPa(m)$^{1/2}$ to the material. This calculation was done assuming the matrix is completely elastic, no plasticity is taken into account, therefore this calculated improvement is an overestimate. Also according to this model increasing the amount of austenite present in the material would also increase the toughness. However, work done by Kim [7] who overtempered 6 Ni steel found that increasing the amount

of austenite present beyond some critical amount does not raise the toughness but in fact raises the DBTT.

It is possible, however, that the austenite transforming to create regions of residual compression will assist in toughening for the fracture process is not a simple one and effects will overlap. On the other hand the fracture surface refinement was most definitely observed, and this is good experimental evidence that the crystallographic cleavage imparement model of precipitated austenite transforming to martensite appears to be a valid one in this 8Ni-2Mn-0.1Ti steel.

CONCLUSIONS

The introduction of precipitated austenite to the matrix of an 8Ni-2Mn-0.1Ti ferritic steel improved the cryogenic mechanical properties by lowering the DBTT but kept the upper shelf energies constant.

The as quenched (Q) specimens fractured in an intergranular manner that was found to be due to an enrichment of P at the grain boundaries. The heat treatments that involved intercritical annealing and tempering eliminated intergranular fracture by causing the P to segregate off the grain boundaries into the austenite.

The austenite that formed in the matrix during tempering was found to lie along (110) planes in the K-S and N-W orientation relationships. The austenite that was thermally stable was found to be so due to it being solute rich. During intercritical tempering and annealing it was found that the matrix polygonizes and goes through various stages of recovery.

The addition of thermally stable precipitated austenite was found to reduce the median facet size by almost half from specimens that contained no austenite. Also the number of large facets is decreased by adding austenite which could be an indication that the cleavage stress is related to the number of large facets. This result seems to be in accord with the crystallographic cleavage impairment model where the austenite transforms to a variant of martensite that differs from the matrix and this effectively grain refines the steel and raises the cleavage stress, and thus increases the toughness.

By intercritical tempering and annealing the yield strengths of the specimens varied according to heat treatment. This was thought to be due to changes in the dislocation density in the specimens created by

the polygonization and recovery process. It was found that an intercritical anneal had a lower yield strength than a longer intercritical temper. This is interesting because the intercritical anneal had a higher DBTT than the temper. This anomaly was thought to be due to the presence of austenite formed in the intercritical temper raised the cleavage stress in fracture and thus toughened the steel.

REFERENCES

1. H. I. McHenry, R. P. Reed: Nuclear Engineering and Design, 58, (1980), North Holland Publishing Co., p. 219.
2. T. Horiucho, R. Ogawa, M. Shimada, S. Tore, M. Yamaga, Y. Kasamatsu: Advances in Cryogenic Engineering Materials, 28, (1982), p. 93.
3. R. Ogawa, J. W. Morris Jr.: Proceedings of the ICMC, Colorado Springs CO, (1983), to be published.
4. W. Jolley: JISI, 206, (1969), p. 170.
5. W. C. Leslie, R. J. Sober, S. G. Babcock, S. J. Green: Trans. ASM, 62, (1969), p. 690.
6. G. R. Spiech, P. R. Swann: JISI, 203, (1965), p. 480.
7. J. I. Kim, PhD thesis, University of California, Berkeley.
8. S. Jin, J. W. Morris Jr., V. F. Zackay: Met. Trans., 6A, (1975), p. 141.
9. S. Jin, S. K. Hwang, J. W. Morris Jr.: Met. Trans., 6A, (1975), p. 1569.
10. S. Jin, S. K. Hwang, J. W. Morris Jr.: Met. Trans., 6A, (1975), p. 1721.
11. C. Syn, S. Jin, J. W. Morris Jr.: Met. Trans., 7A, (1976), p. 1827.
12. S. Jin, J. W. Morris Jr., V. F. Zackay, Technical report no. 2, Office of Naval Research, Contract no. N00014-69-A-0200-1062, NR031-762.
13. H. J. Rack, D. Kalish: Met. Trans., 2, (1971), p. 3011.
14. C. N. Alquist: Acta. Met., 23, (1975), p. 239.
15. O. Tamate: Int. J. Frac. Mech., 4, (1968), p. 257.
16. S. Antolovich, B. Singh: Met. Trans., 2, (1971), p. 2135.

17. W. W. Gerberich, P.L. Hemmings, V. F. Zackay, E. R. Parker: Fracture, (1969), Chapman and Hall, London, p. 228.

18. J. I. Kim, J. W. Morris Jr.: Met. Trans., 11A, (1980), p. 1401.

19. C. W. Marshal, R. H. Hehemann, A. R. Triano: Trans. ASM, 55, (1962), p. 135.

20. J. W. Morris Jr., C. K. Syn, J.I. Kim, B. Fultz: Proceedings of the International Conference on Martensitic Transformations, MIT, Cambridge Mass., (1979), p. 572.

21. G. R. Brophy, A. J. Miller: Trans. ASM, 41, (1949), p. 1185.

22. S. D. Antolovich, A. Saxena, G. R. Chanai: Met. Trans., 5A, (1974), p. 623.

23. G. Y. Lai, W. E. Wood, R. A. Clark, V. F. Zackay, E. R. Parker: Met. Trans., 5A, (1974), p. 1663.

24. J. I. Kim, C. K. Syn, J. W. Morris Jr.: Met. Trans., 14A, (1983), p. 93.

25. S. K. Hwang, Masters Thesis, University of California, Berkeley.

26. B. Fultz, Masters Thesis, University of California, Berkeley.

27. K. J. Kim, L. H. Schwartz: Mater. Sci. Eng., 33, (1978), p. 5.

28. B. P. J. Sandvik, C. M. Wayman: Met. Trans., 14A, (1983), p. 809.

29. J. P. Naylor: Met. Trans, 10A, (1979), p. 861.

30. U. H. Lindbad, B. L. Averbach: Acta. Met., 14, (1966), p. 1583.

31. J. P. Naylor, P. R. Krahe: Met. Trans., 6A, (1975), p. 594.

32. M. J. Roberts: Met. Trans., 1, (1970), p. 3287.

33. S. Yano, H. Sakurai, H. Mimura, N. Wakita, T. Ozawa, K. Aori: Trans. ISIJ, 13, (1973), p. 133.

34. R. L. Miller: Trans. ASM, 57, (1964), p. 892.

35. A. Boyd, P. G. T. Howell: Scanning Electron Microscopy, 1, (1977), p. 571.

36. G. O. Fior, Masters Thesis, University of California, Berkeley.

37. H. J. Kim, PhD Thesis, University of California, Berkeley.

38. J. M. Rigsbee: Proceedings of the International Confernece on Martensitic Transformations, MIT, Cambridge Mass., (1979), p. 381.

39. K. W. Andrews: JISI, 203, (1965), p. 721.

40. S. Jin, S. K. Hwang, J. W. Morris Jr.: Technical report no. 6, Office of Naval Research, Contract no. N00014-69-A-0200-1062, NR031-762.

41. H. Ohtani, H. G. Feng Jr., C. J. McMahon: Met. Trans., 7A, (1976), p. 1123.

42. C. J. McMahon: Mater. Sci. Eng., 25, (1976), p. 233.

43. G. R. Brophy, A. J. Miller: Trans. ASM, 41, (1949), p. 1185.

44. H. J. Kim, J. W. Morris Jr., to be published.

45. B. Fultz, J. I. Kim, J. W. Morris Jr., to be published.

46. B. Kurdjomov, G. Sachs: Z. Physik, 64, (1930), p. 325.

47. Z. Nishiyama: Martensitic Transformations, (1978), Academic Press, New York, p. 8.

48. G. T. Hahn: Acta. Met., 10, (1962), p. 727.

49. R. O. Ritchie: Met. Trans., 8A, (1977), p. 1131.

50. T. Matsuyama, H. Suto: Trans. JIM, 20, (1979), p. 44.

51. S. Yu, C. J. McMahon Jr.: Met. Trans., 11A, (1980), p. 277.

52. H. Lee, PhD Thesis, University of California, Berkeley.

53. J. I. Kim, J. W. Morris Jr.: Technical Report no. 13, Office of Naval Research, contract no. N00014-75-C-0154.

54. G. Hettich, H. Mehrer, K. Muier: Scripta Met., 11, (1977), p. 795.

55. B. Fultz, PhD Thesis, University of California, Berkeley.

56. W. Koch, J Dittman, H. Keller: Arch. Eisenhutenw, 39, (1968), p. 457.

57. K. Faber, PhD Thesis, University of California, Berkeley.

58. R. M. McMeeking, A. G. Evans: Amer. Ceram. Soc., 65, (1982), p. 242.

Table I. Chemical Composition of Fe-8Ni-2Mn Alloy in weight percent.

Ni	Mn	Ti	N	O	P	S	C	Fe
7.95	1.93	0.07	0.003	0.004	0.003	0.003	<0.001	Bal.

Table II. Charpy Impact Data giving shelf energies, Ductile to Brittle Transistion Temperatures, and shifts in DBTT as a function of heat treatment.

Blunt Notch

Sample	DBTT (K)	Upper Shelf Energy (Ft-lb)	(J)	Lower Shelf Energy (Ft-lb)	(J)	Shift from Q (K)	Shift from QL (K)	Shift from QT (K)
Q	269	201	272	2	37	-	-	-
QL	113	199	270	6	8	-156	-	-
QT	108	206	279	8	11	-161	-5	-
QLT	77	208	281	11	15	-192	-36	-31

Sharp Notch

Sample	DBTT (K)	Upper Shelf Energy (Ft-lb)	(J)	Lower Shelf Energy (Ft-lb)	(J)	Shift from Q (K)	Shift from QL (K)	Shift from QT (K)
Q	289	100	136	2	3	-	-	-
QL	205	100	136	2	3	-84	-	-
QT	193	100	136	3	4	-96	-12	-
QLT	138	100	136	6	8	-151	-67	-55

Table III. Tensile Data as a function of heat treatment and testing temperature.

Sample	Testing Temp. (K)	Yield Strength Ksi	Yield Strength GPa	Ultimate Tensile Ksi	Ultimate Tensile GPa	Fracture Stress Ksi	Fracture Stress GPa	% Total Elongation	% Reduction in Area
Q	77	148	1.02	166	1.14	284	1.06	15.0	68.8
	293	114	0.795	117	0.806	208	1.43	9.3	74.0
QL	77	121	0.833	148	1.02	347	2.39	21.0	75.7
	119	104	0.716	120	0.827	225	1.55	16.0	72.0
	178	95	0.654	113	0.779	250	1.72	17.2	72.5
	293	90	0.62	121	0.833	210	1.45	15.0	71.9
QT	77	126	0.465	137	0.946	394	2.71	30.0	79.5
	127	105	0.723	110	0.758	235	1.62	17.6	75.0
	174	102	0.703	117	0.806	250	1.72	24.0	75.7
	293	97	0.668	108	0.744	246	1.69	24.0	77.5
QLT	77	115	0.791	135	0.93	685	4.62	36.0	88.0
	123	97	0.678	113	0.779	261	1.8	23.0	77.7
	169	85	0.585	105	0.723	222	1.53	27.0	75.1
	293	82	0.565	92	0.633	176	1.21	26.0	76.7

Table IV. Chemical composistions of precipitated austenite, and matrix, as detected by EDAX in STEM for QLT heat treatment.

Element	Nominal Composition (wt. %)	Matrix (wt. %)	γ (wt. %)
Fe	90	89.7	80.8
Ni	8	7.2	13.3
Mn	2	3.1	5.9

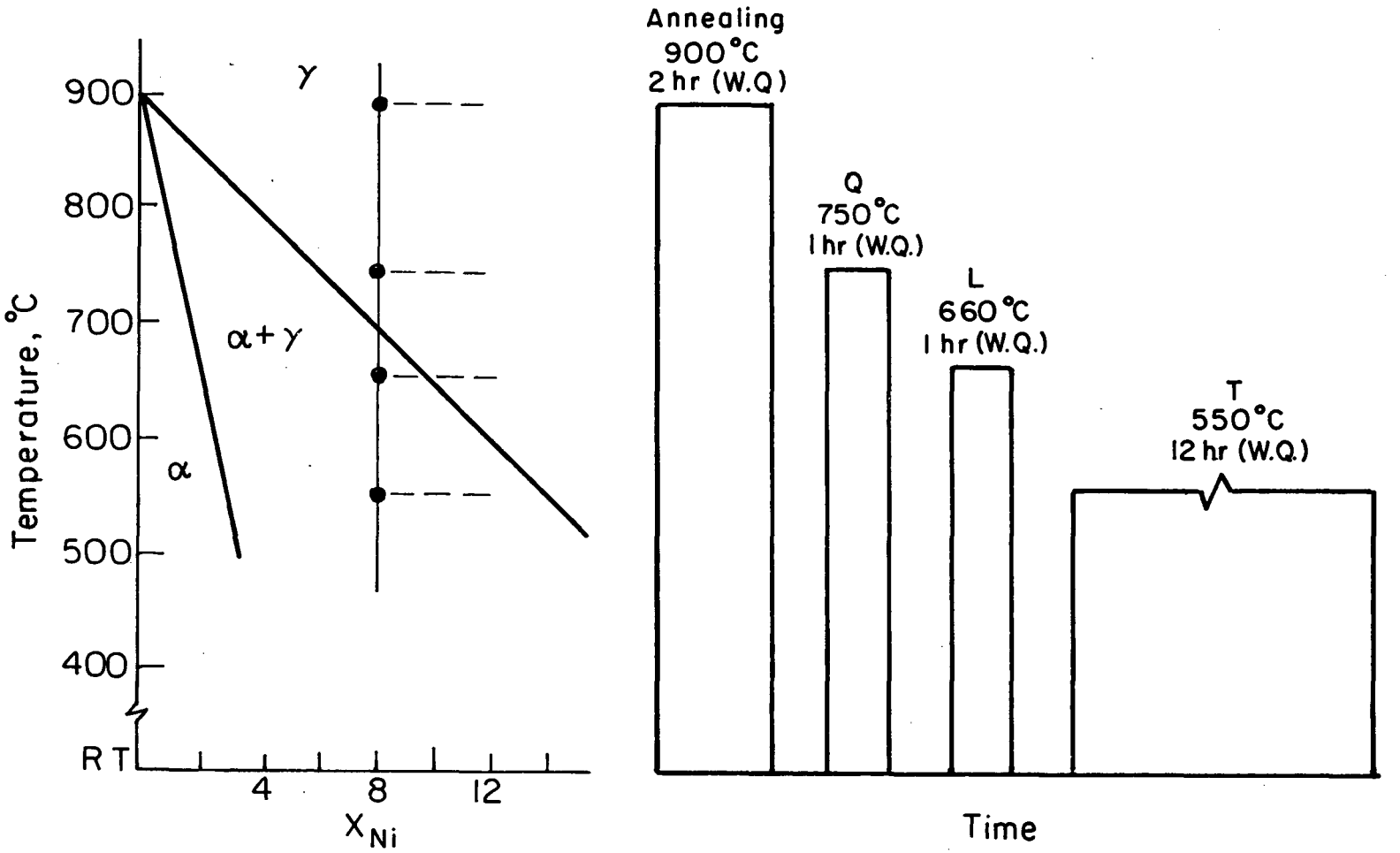

Fig. 1. Schematic diagram showing heat treatment times and temperatures along with the relevant portion of the phase diagram.

XBL 8310-6533

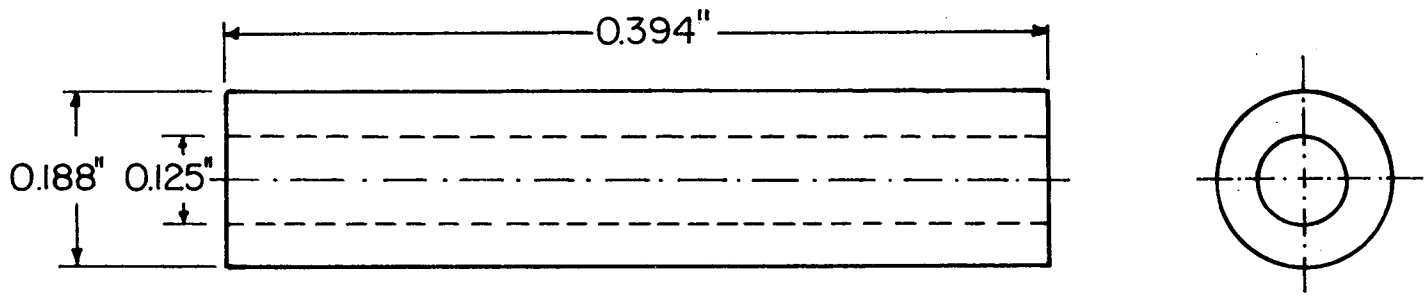

Fig. 2. Dilatometry specimen used to measure phase transformation temperature (1 inch = 25.4 mm).

XBL 7910-7192

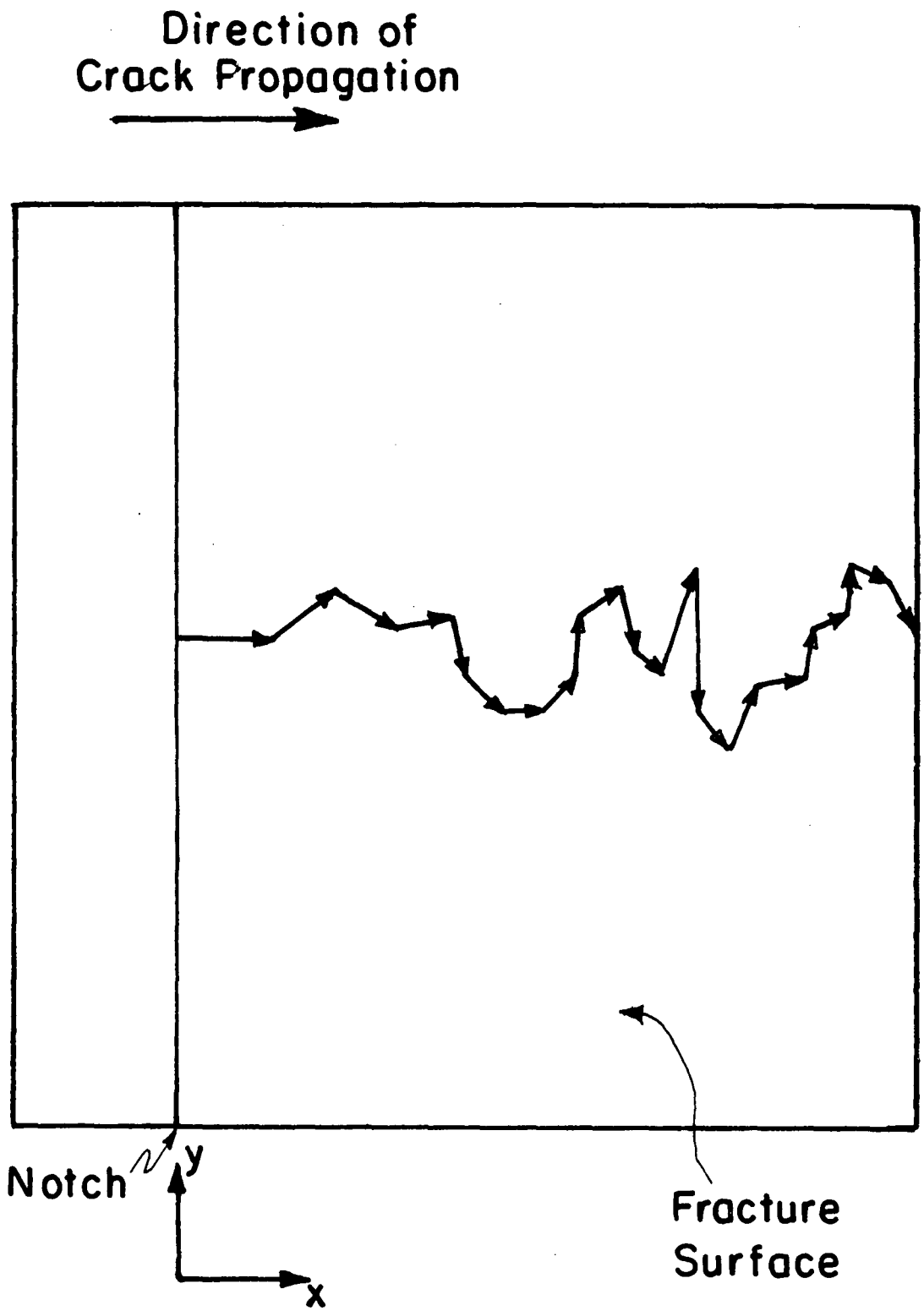

Fig. 3. Schematic diagram of random process by which SEM stereo pair photographs were taken across a broken brittle Charpy specimen.

XBL 844-6839

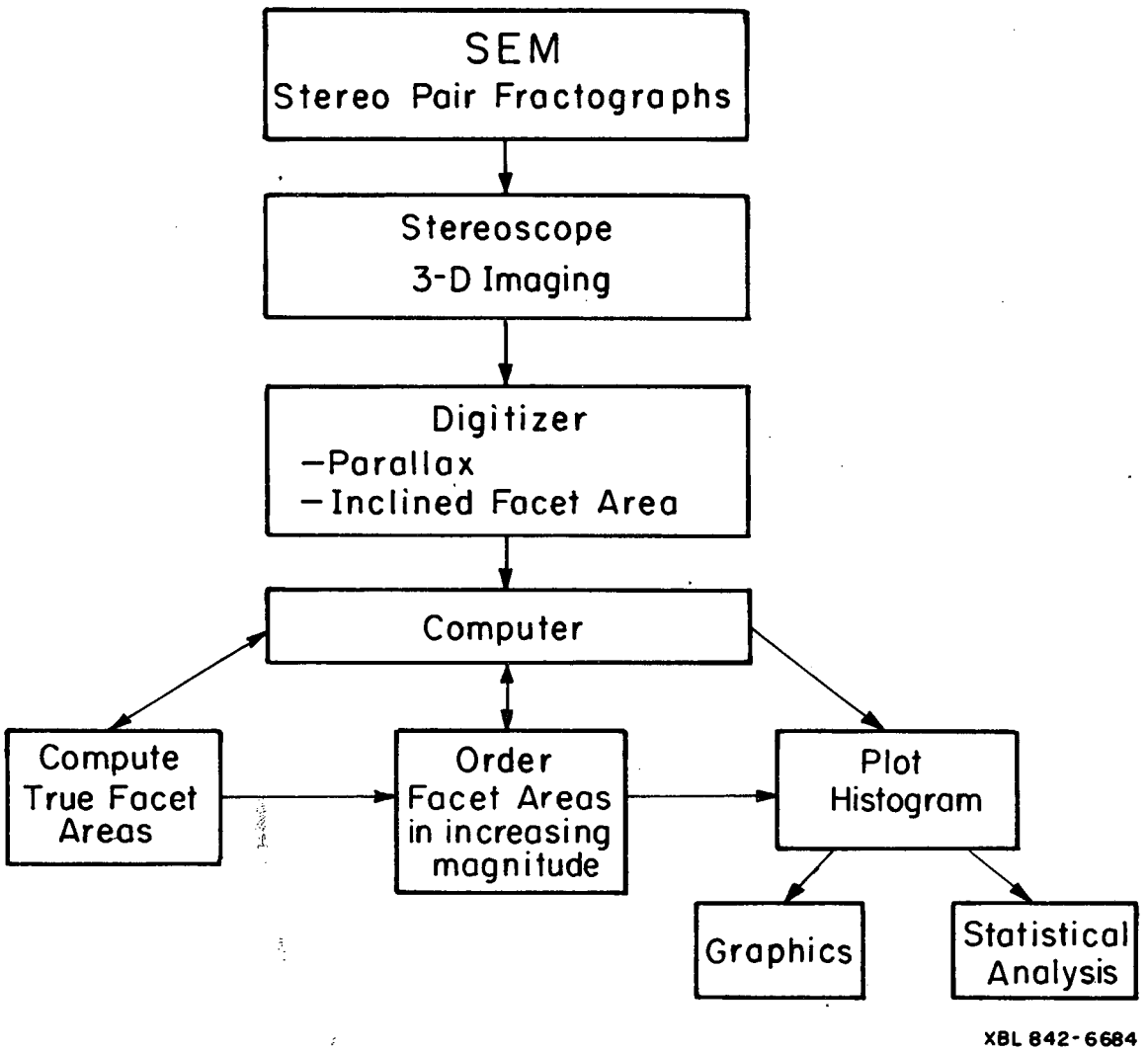

Fig. 4. Flow chart showing the process of measuring facet size in 3D.

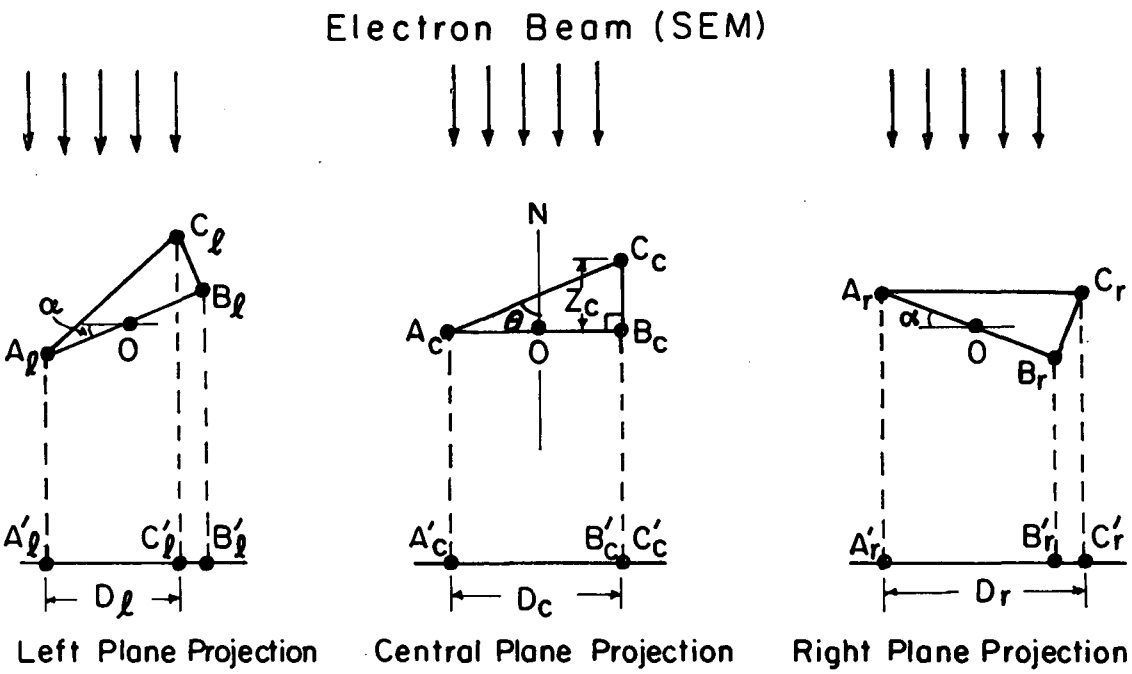

$$D_r - D_\ell \equiv \text{"Paralax" } P$$

$$D_\ell = D_c \cos\alpha - Z_c \sin\alpha \qquad D_r = D_c \cos\alpha + Z_c \sin\alpha$$

$$D_r - D_\ell \equiv Z_c 2 \sin\alpha$$

$$\boxed{Z_c = \frac{P}{2\sin\alpha}}$$

$$\tan\theta = \frac{Z_c}{A'_\ell C'_\ell}$$

$$\theta = \tan^{-1}\left(\frac{Z_c}{A'_\ell C'_\ell}\right)$$

$$\text{True Area} = (\text{Inclined Area})\cos\theta$$

Fig. 5. Geometry of tilting specimen in SEM to create 3D image. XBL 8310-6539

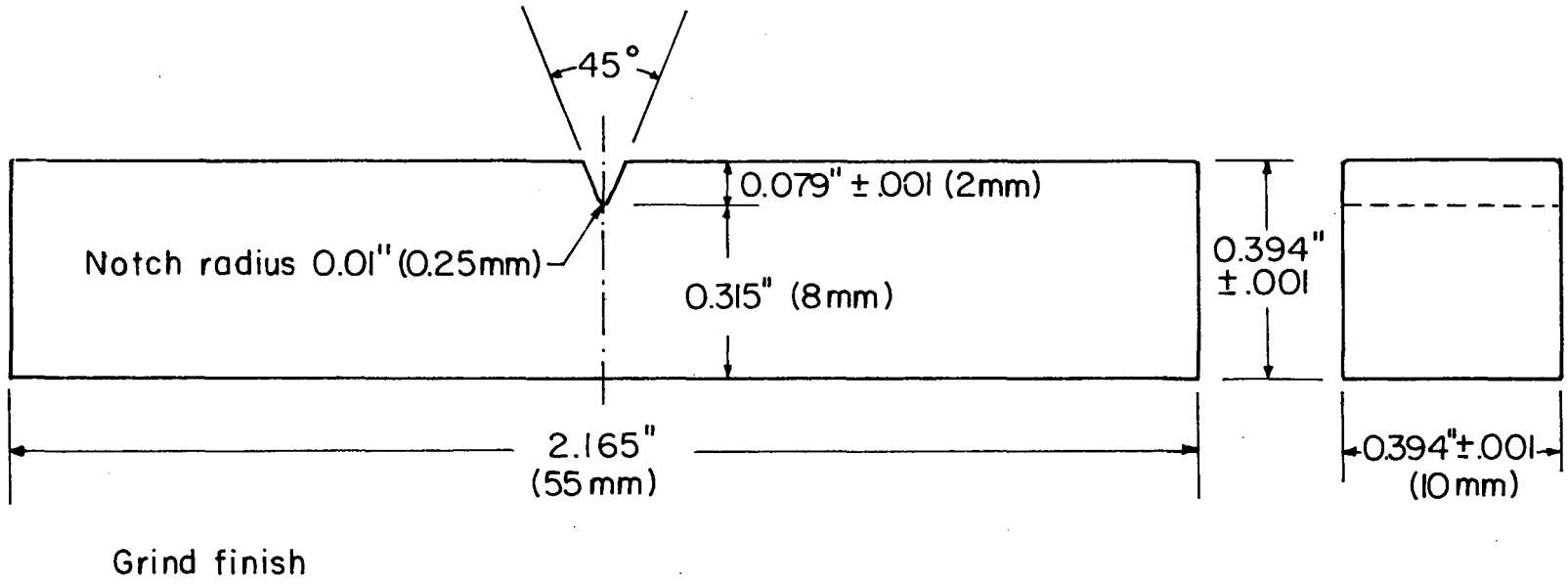

Fig. 6. Standard Charpy test specimen.

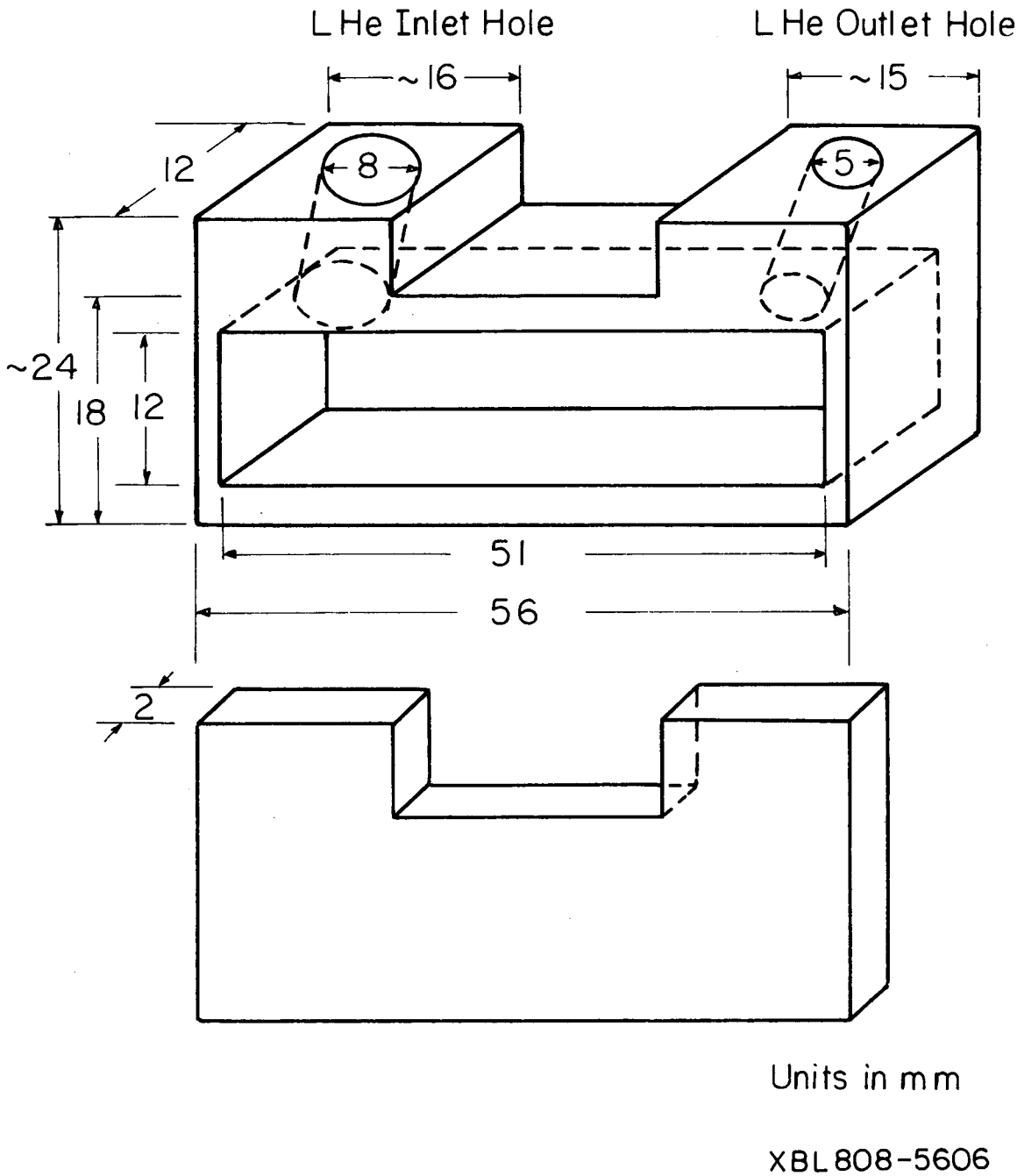

Fig. 7. Styrofoam box used to insulate Charpy specimens for liquid helium testing.

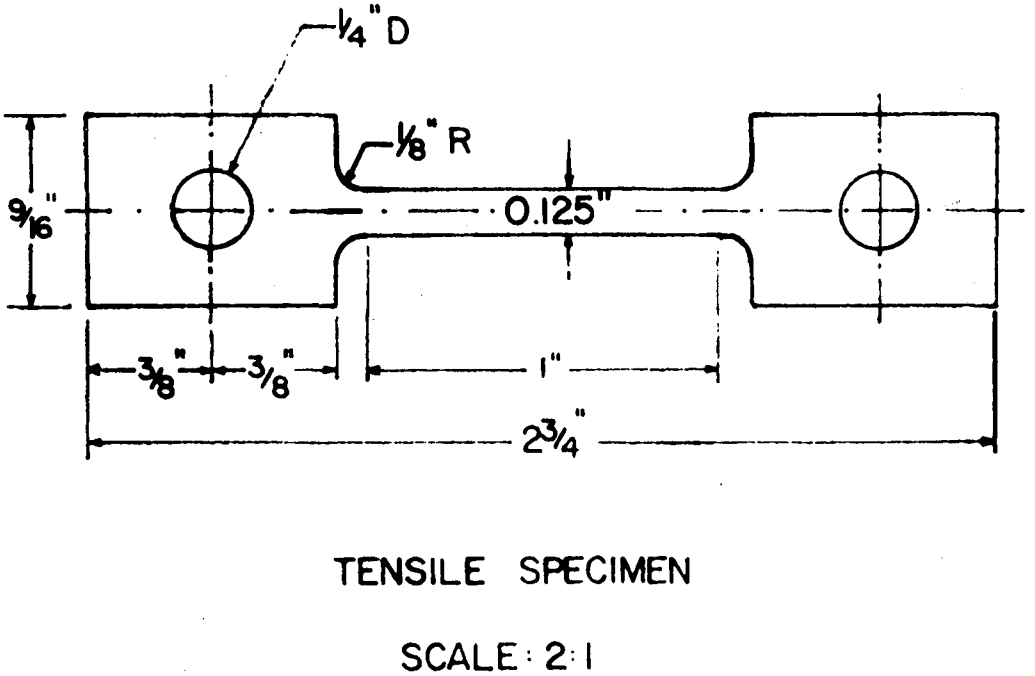

XBL 698-1155

Fig. 8. Subsize flat tensile specimen.

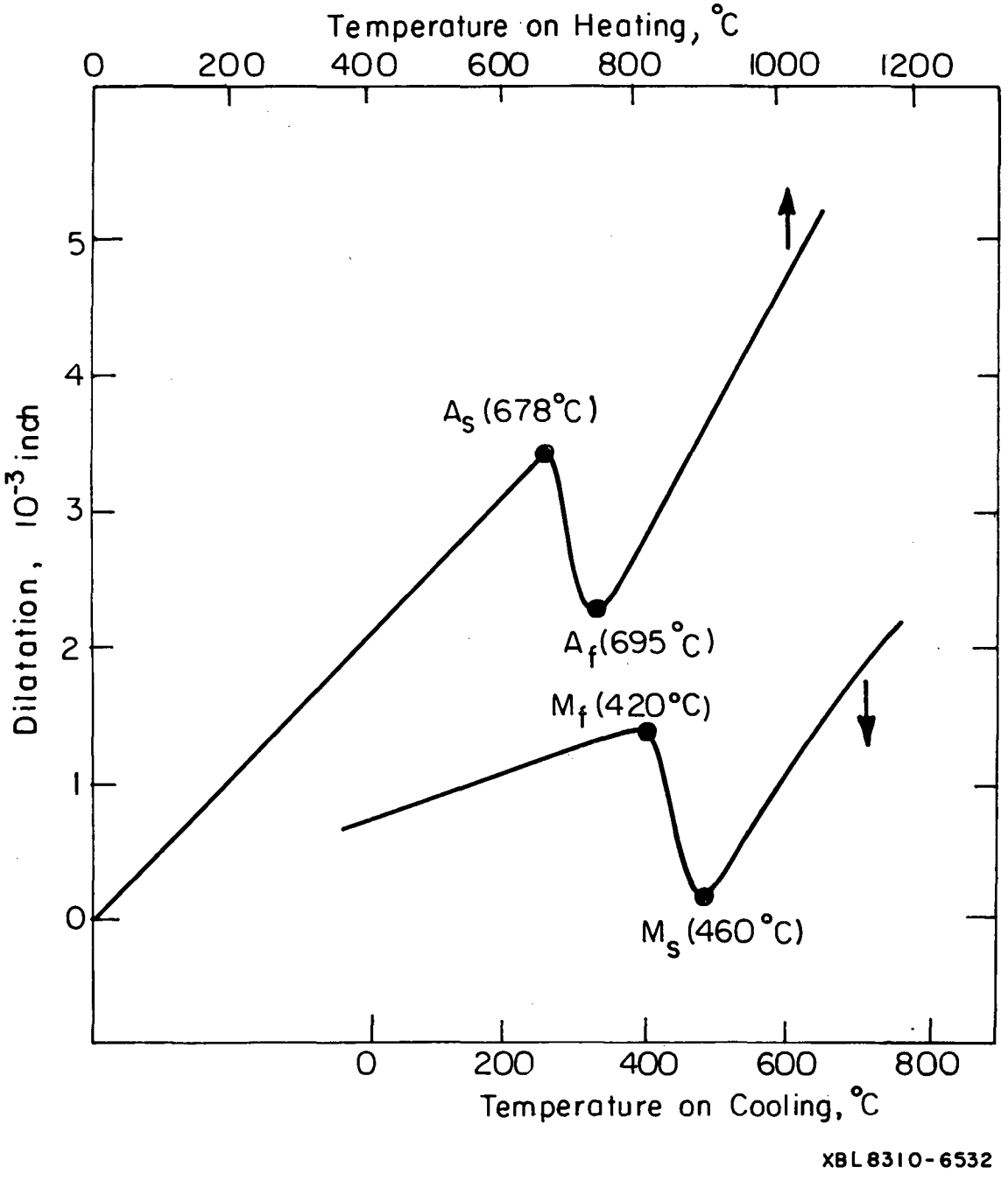

Fig. 9. Dilatometry curves showing A_s and A_f on heating and M_s and M_f on cooling.
(10^{-3} inch = 25.4 μm)

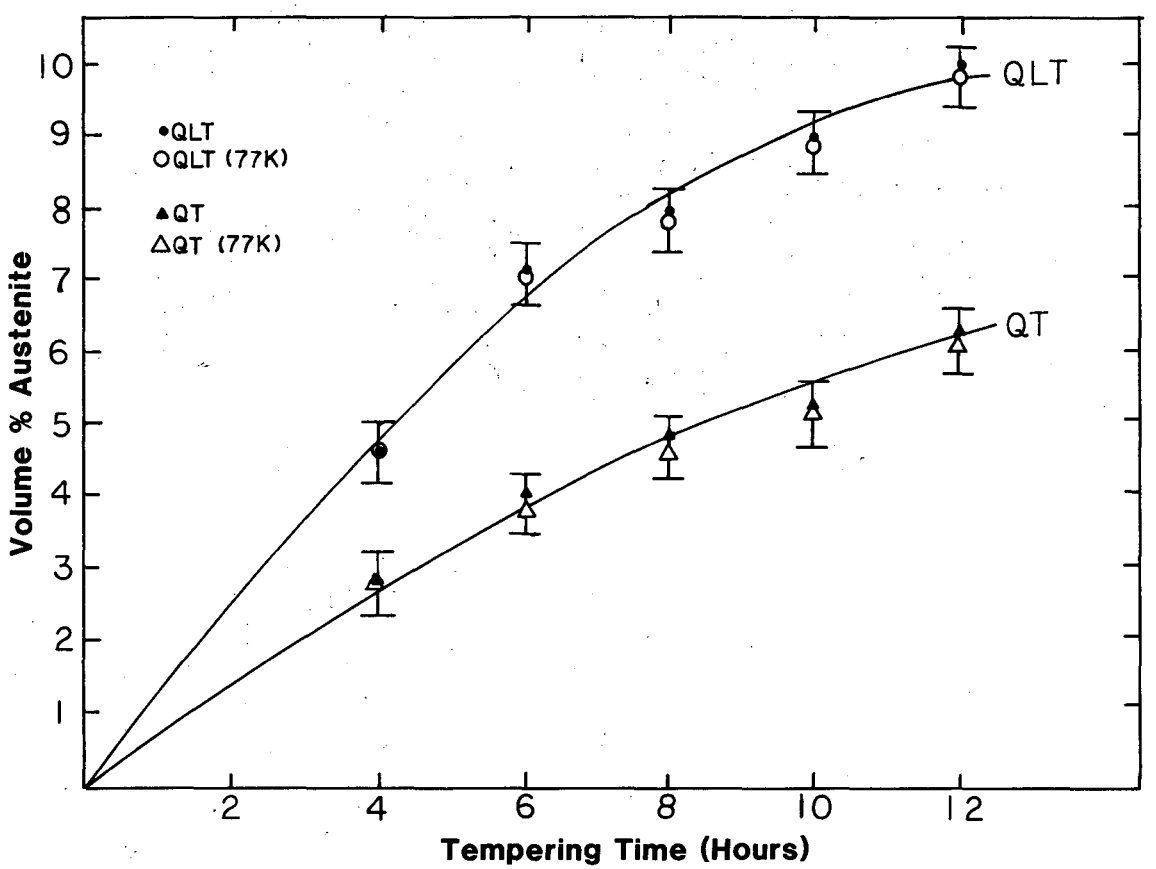

XBL 844-1440

Fig. 10. Volume % precipitated austenite as a function of tempering time for QT and QLT, both at room temperature and after a liquid nitrogen quench.

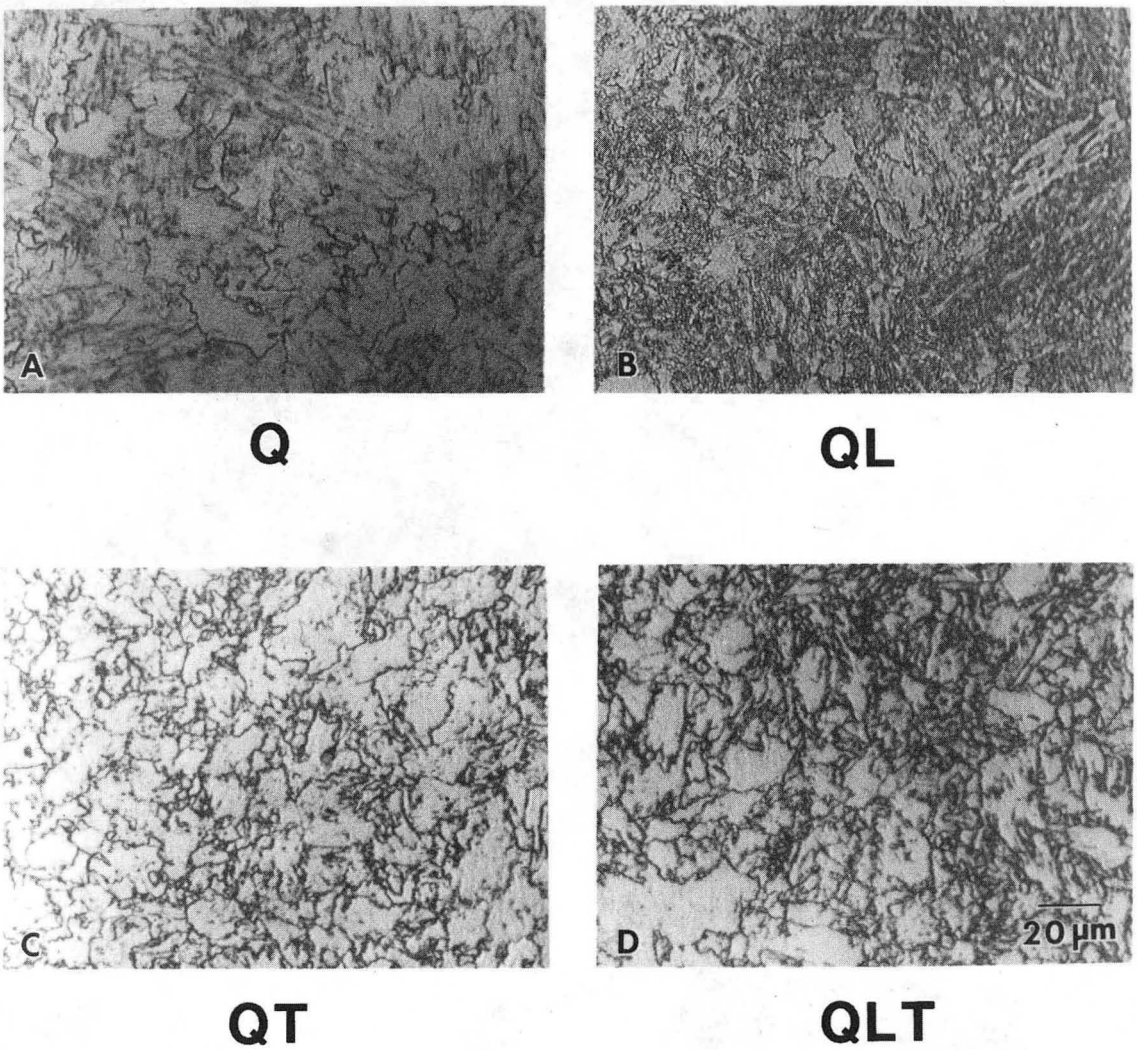

Fig. 11. Optical micrographs of specimens as a function of heat treatment. Nital etch.

XBB 830-11085

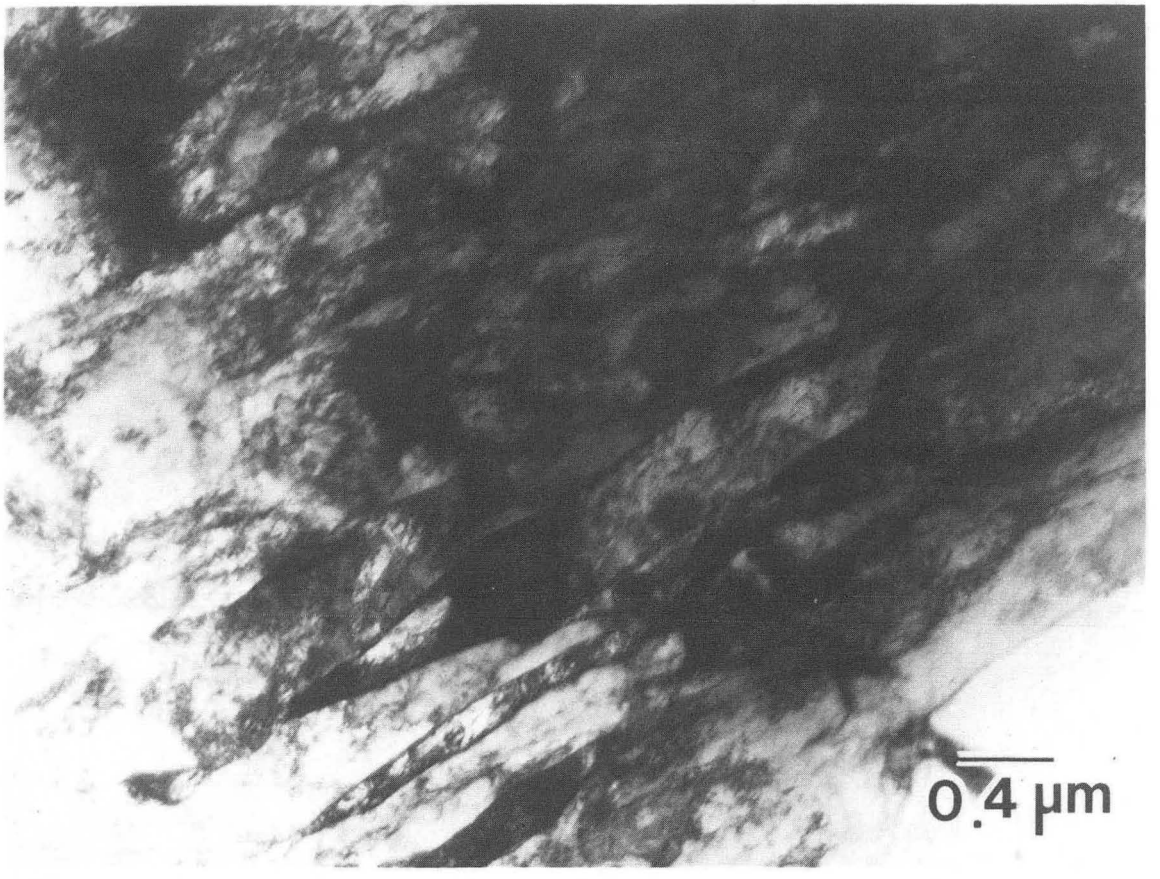

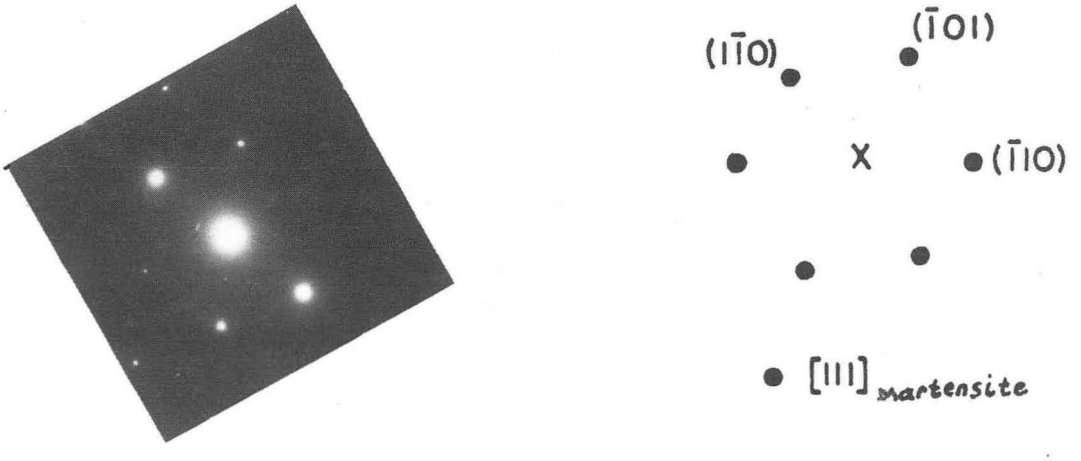

Fig. 12. TEM micrograph showing typical lath microstructure of the Q heat treatment.

XBB 830-11088

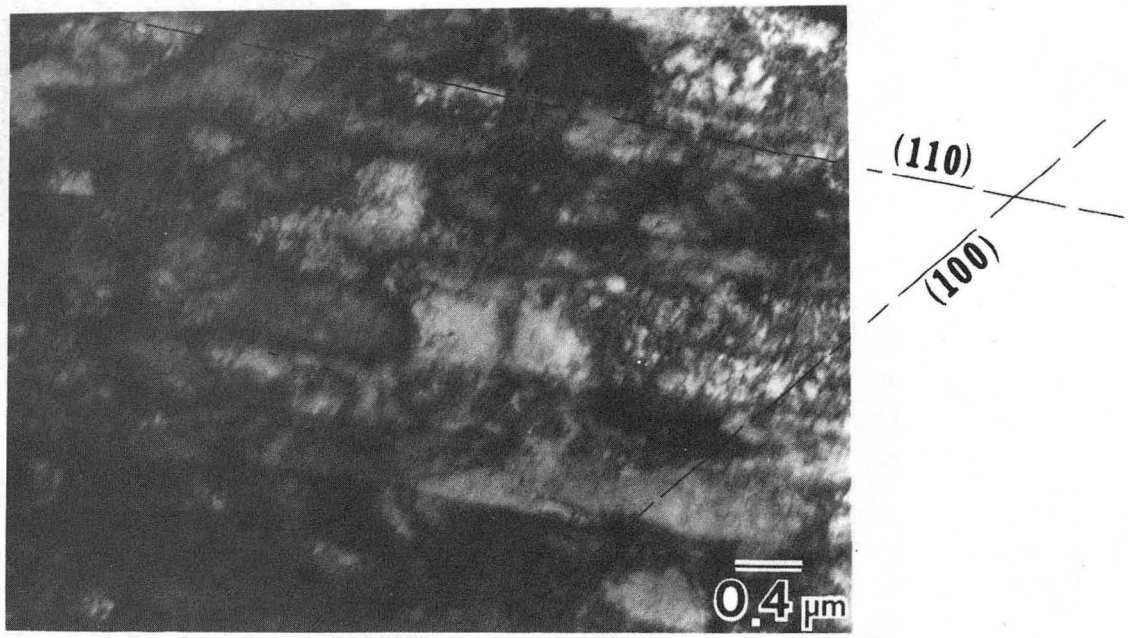

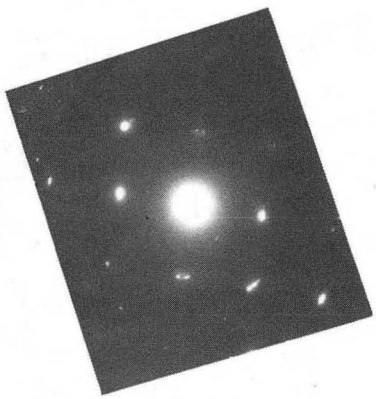

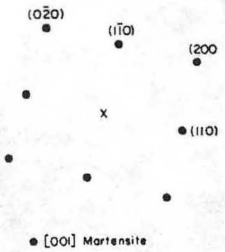

Fig. 13. TEM micrograph of lath microstructure showing (110) lath plane and (100) cleavage plane.

XBB 830-11082

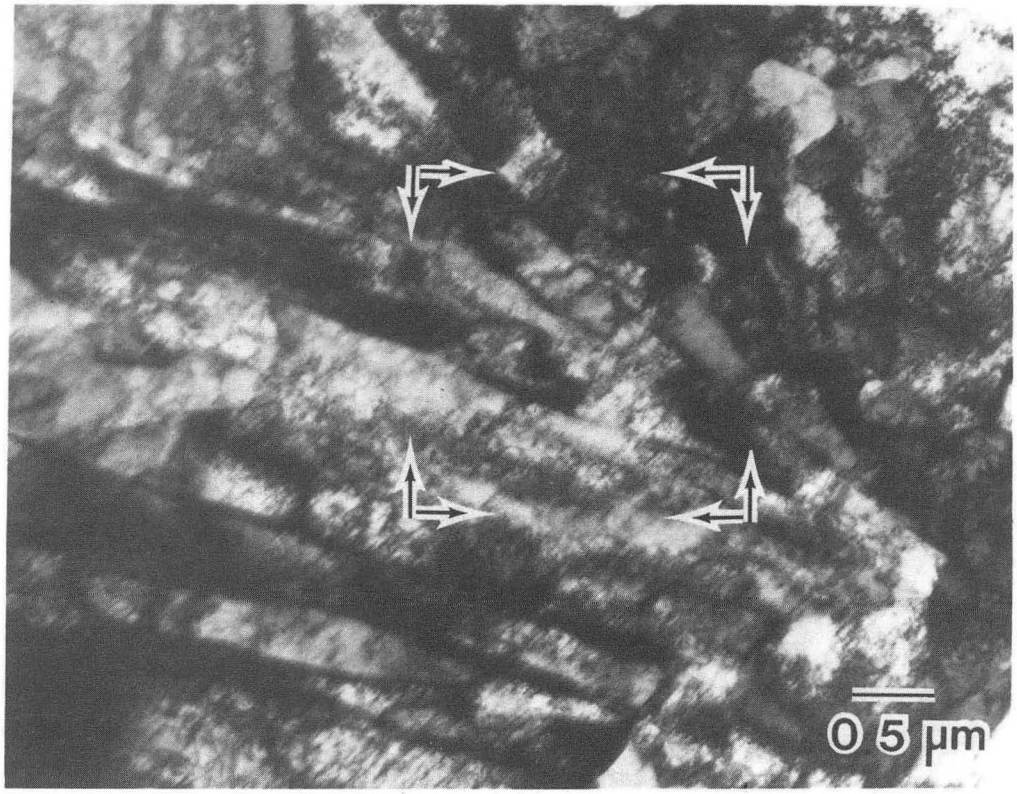

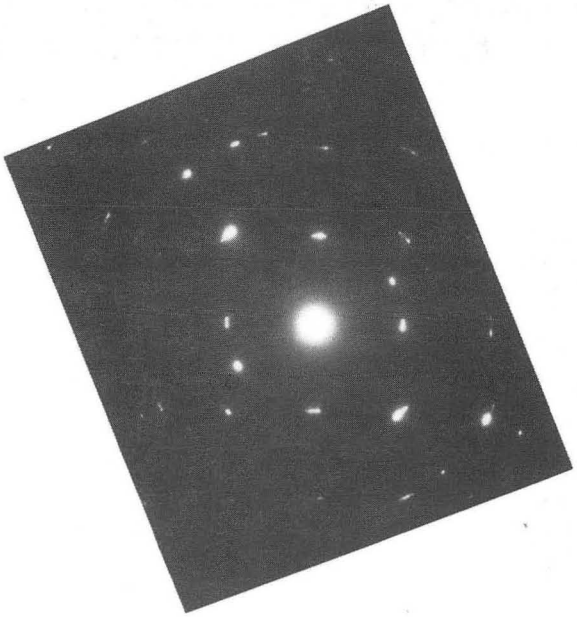

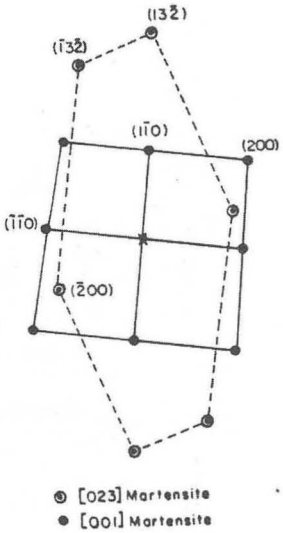

Fig. 14. TEM micrograph of Q condition showing a boundary. Diffraction pattern form area bounded by arrows.

XBB 830-11083

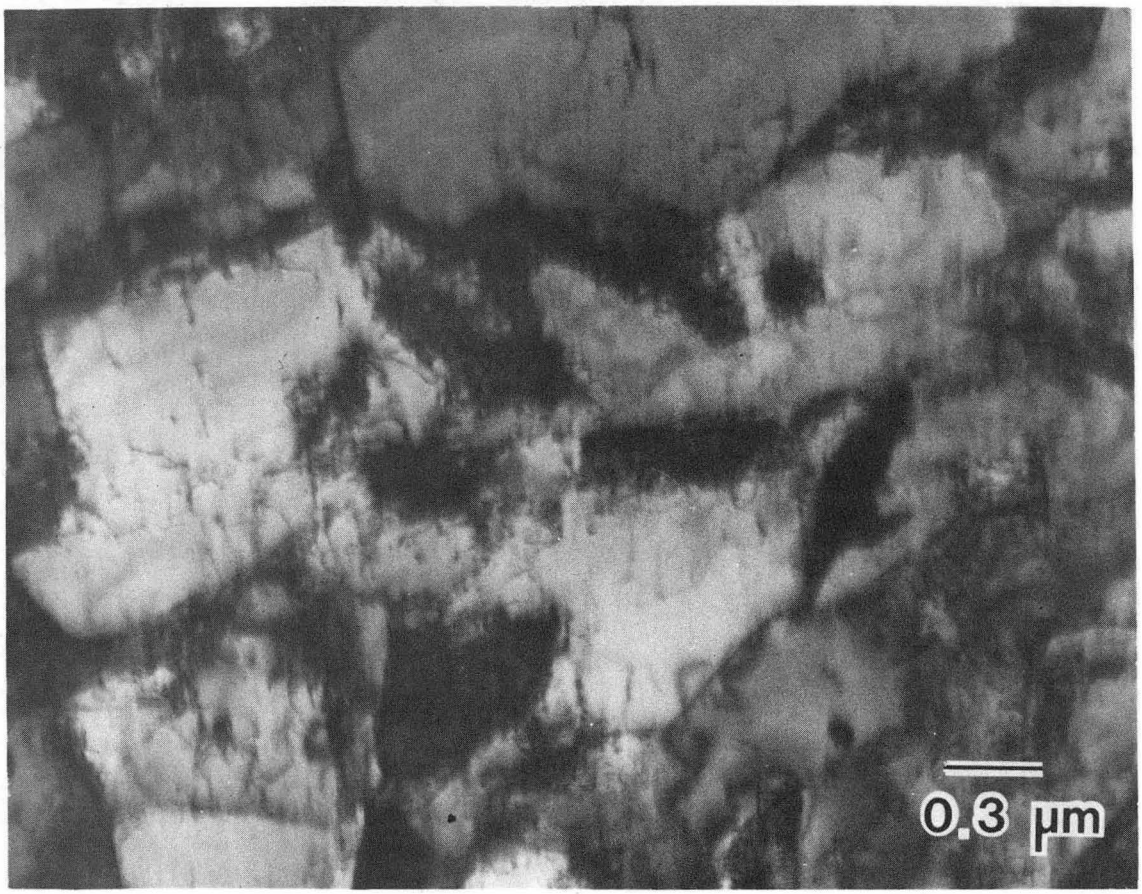

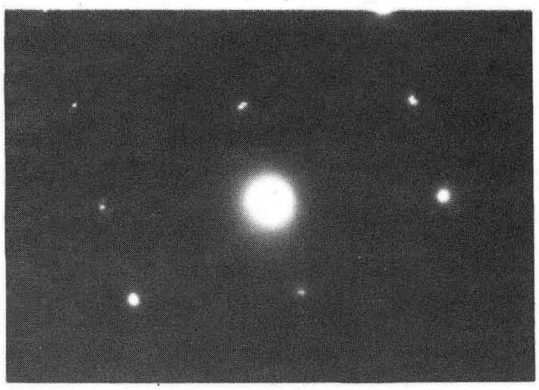

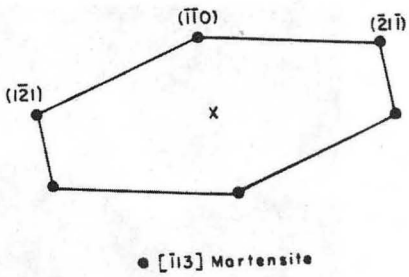

Fig. 15. TEM micrograph of QL specimen.

XBB 830-11081

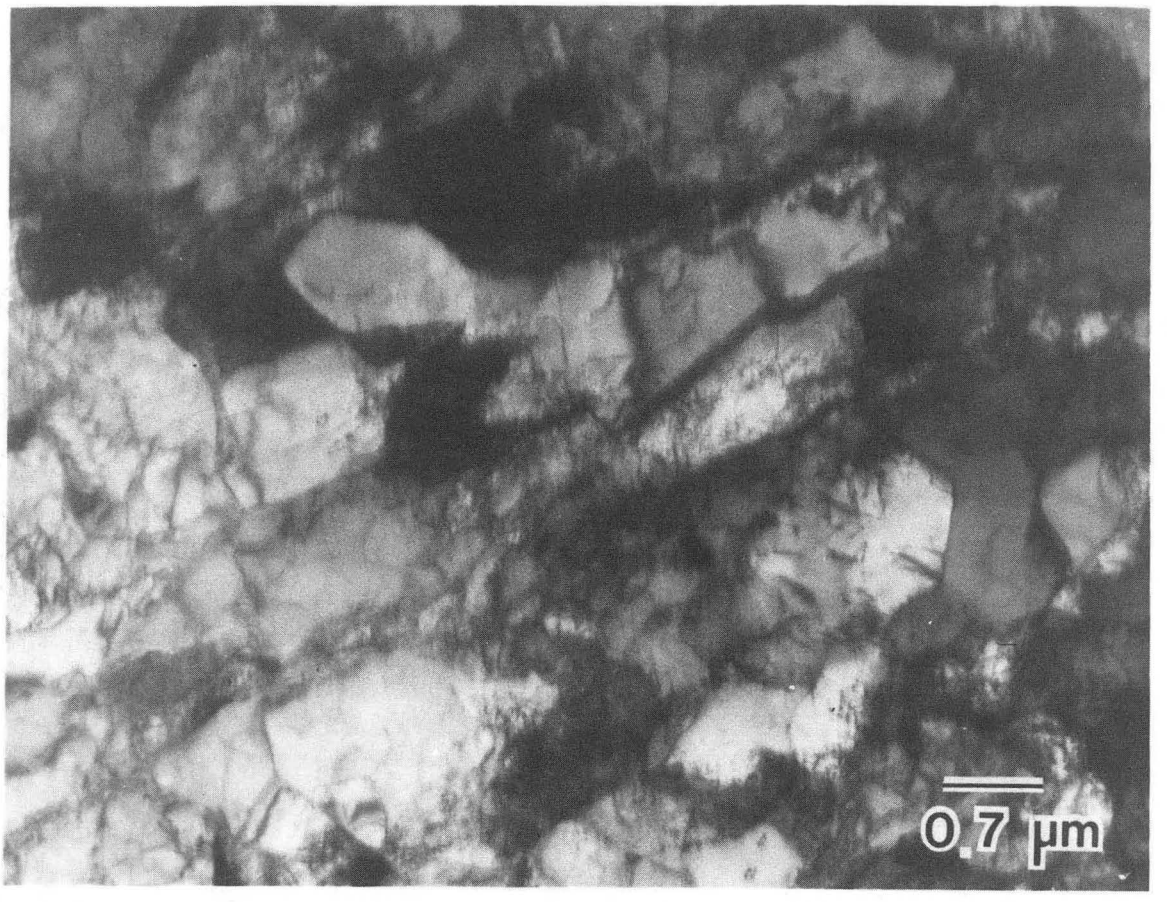

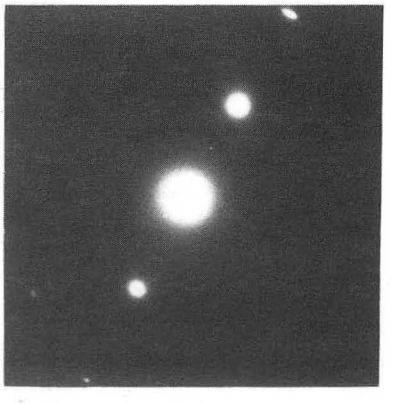

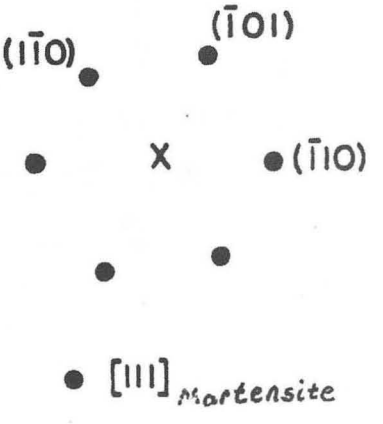

Fig. 16. TEM micrograph of QL specimen.

XBB 830-11086

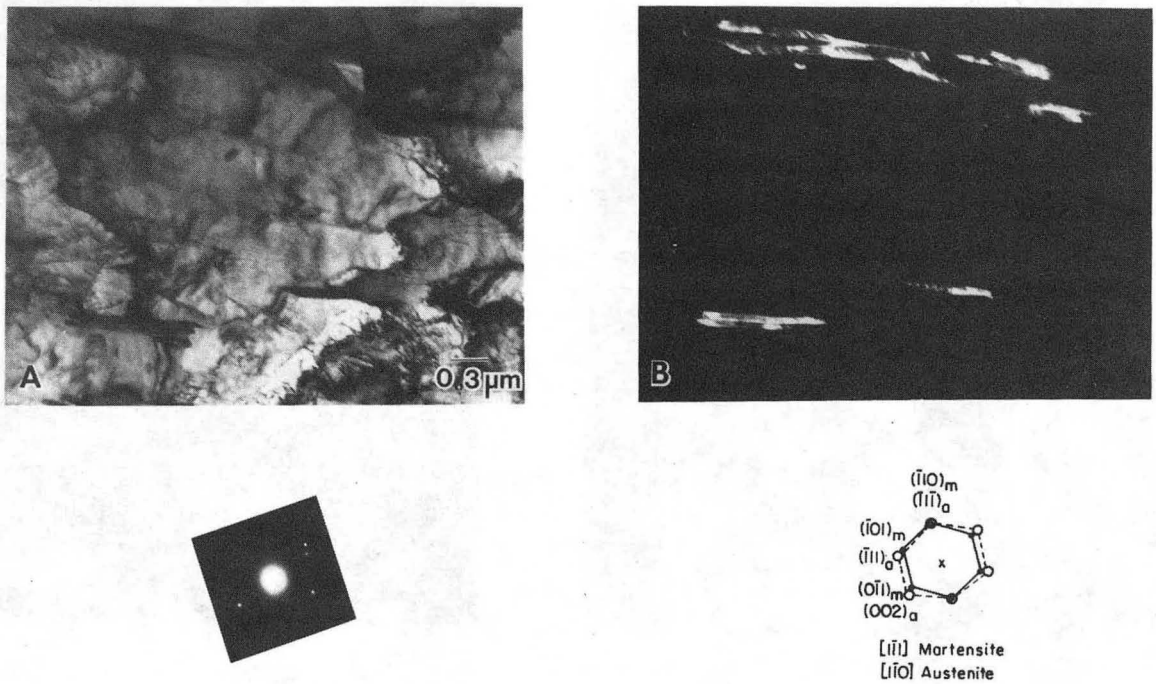

Fig. 17. TEM micrograph of QT specimen, A)Bright Field image B)Dark Field contrast of austenite.

XBB 843-1581

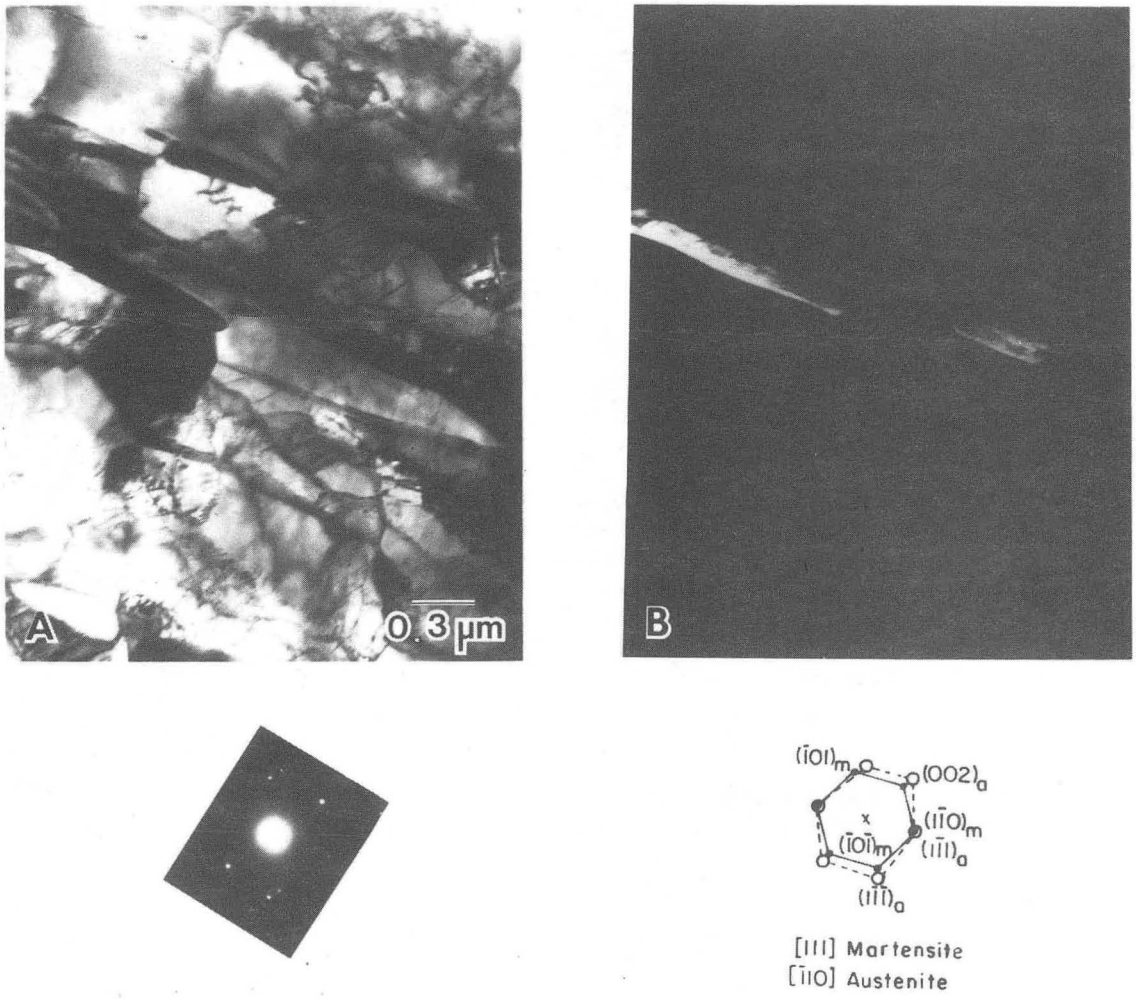

Fig. 18. TEM micrograph of QT specimen, A)Bright Field image B)Dark Field contrast of austenite particle.

XBB 843-1580

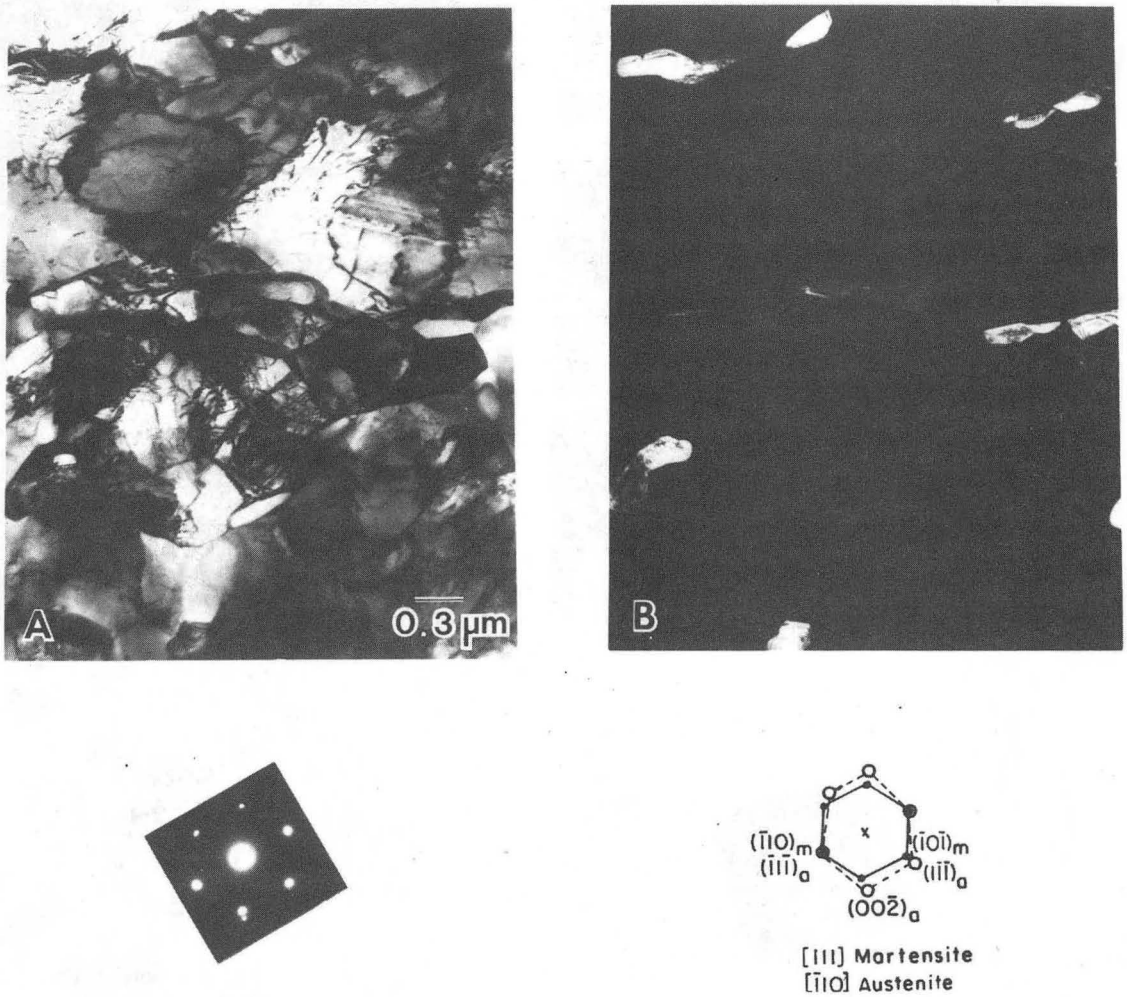

Fig. 19. TEM micrograph of QT specimen A)Bright Field image B)Dark Field contrast of austenite oriented inclined to beam.

XBB 843-1583

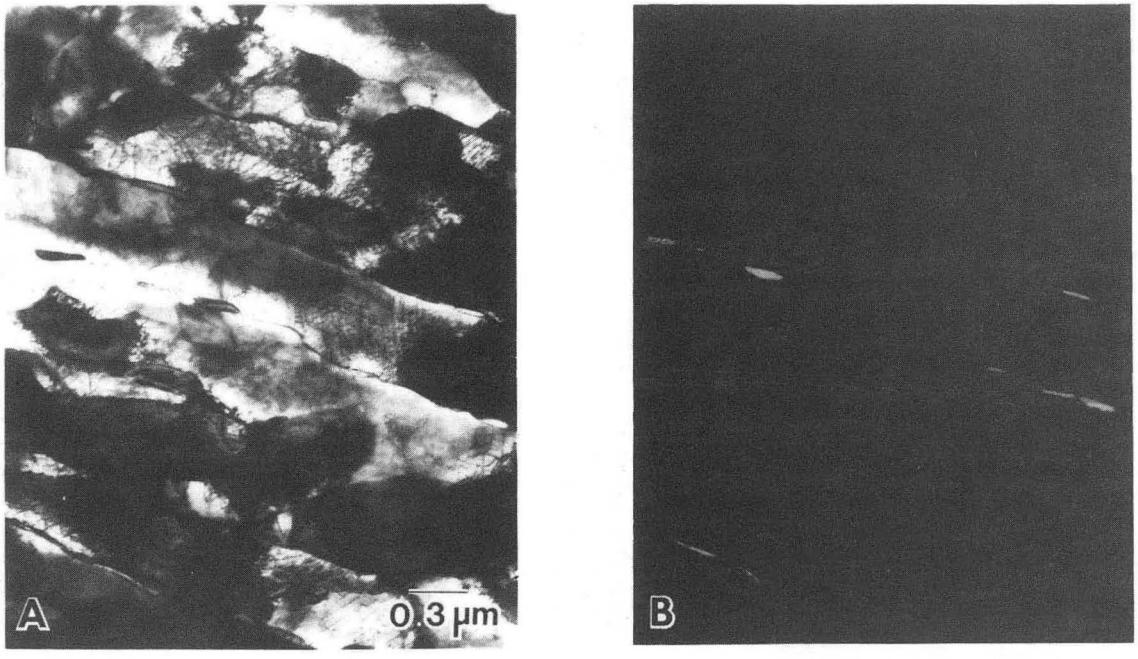

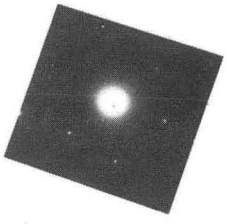

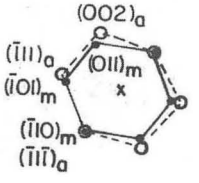

[111] Martensite
[110] Austenite

Fig. 20. TEM micrograph of QT specimen A)Bright Field image showing lath structure B)Dark field contrast of precipitated austenite.

XBB 843-1582

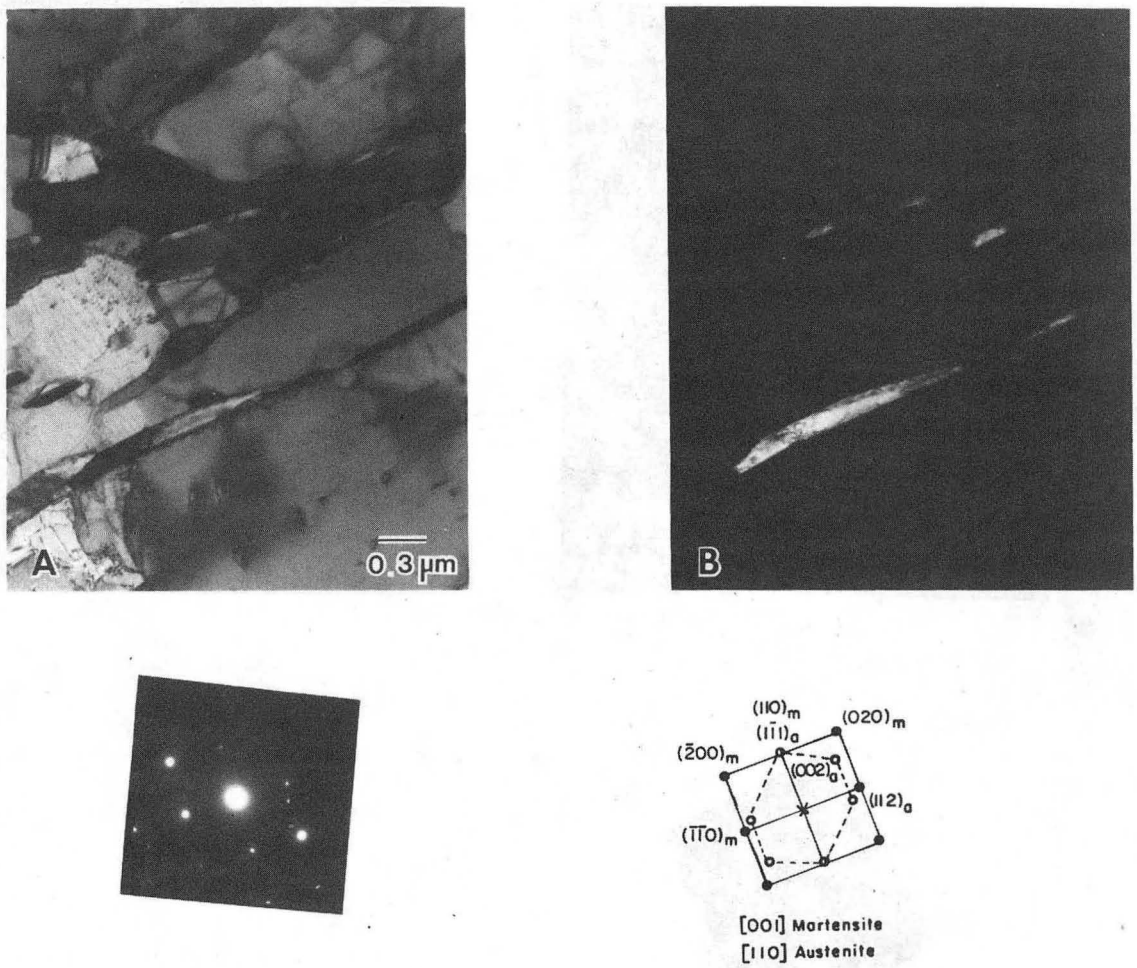

Fig. 21. TEM micrograph of QLT specimen A)Bright Field image B)Dark Field contrast of austenite.

XBB 830-11090

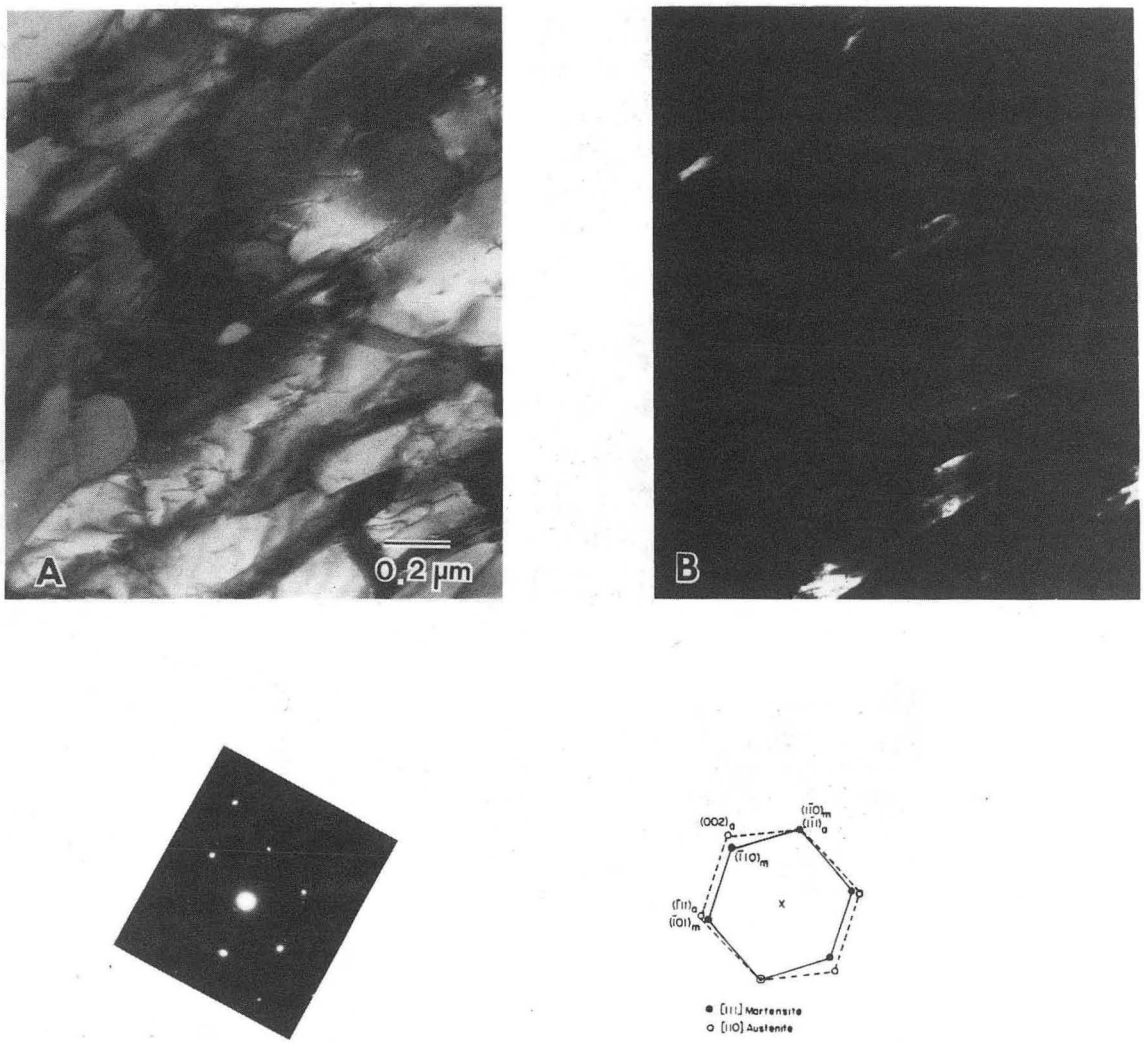

Fig. 22. TEM micrograph of QLT specimen A)Bright Field image B)Dark Field contrast of austenite.

XBB 830-11079

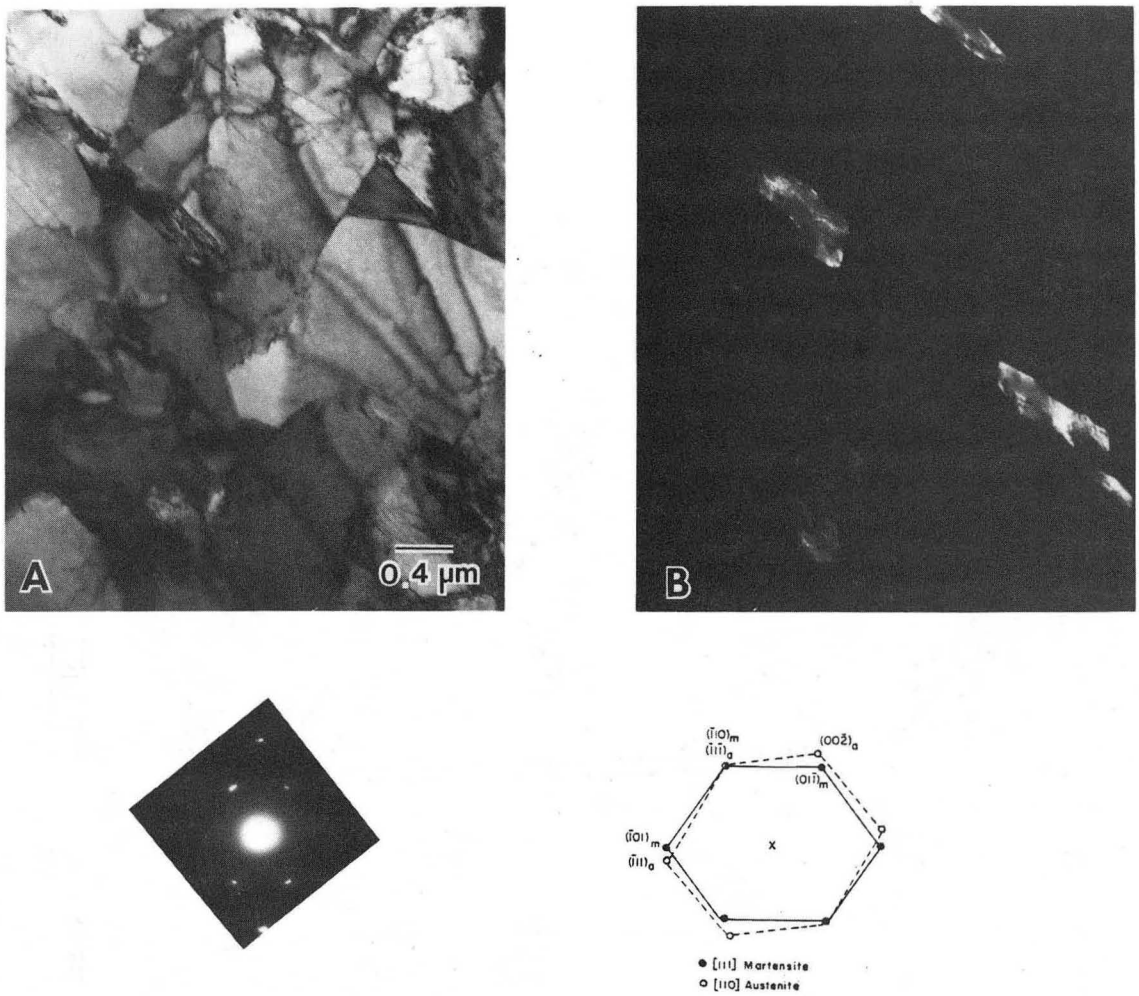

Fig. 23. TEM micrograph of QLT specimen A)Bright Field image B)Dark Field contrast of precipitated austenite oriented inclined to the beam.

XBB 830-11078

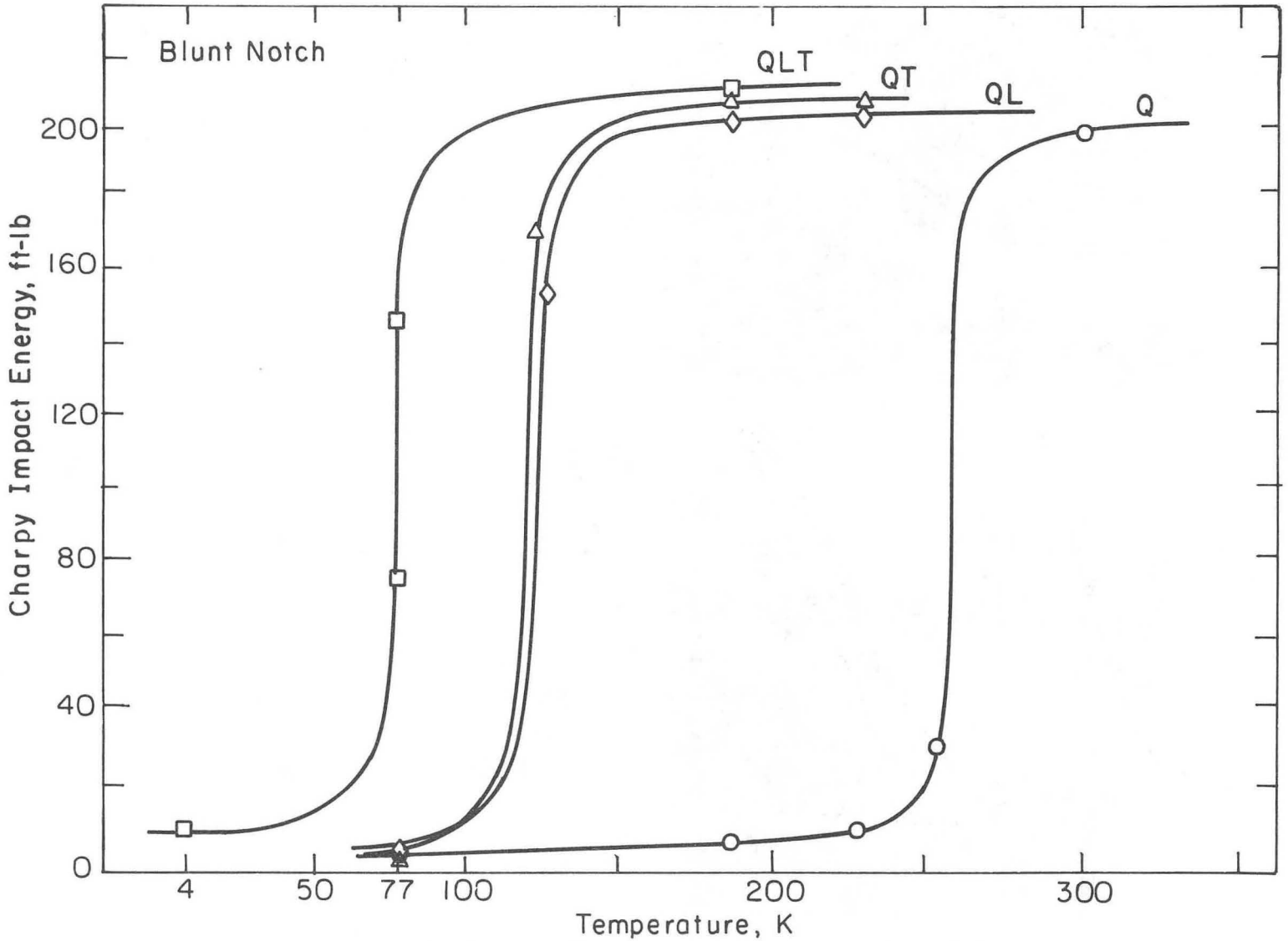

Fig. 24. Ductile-to-Brittle Transition curves as a function of heat treatment for blunt notch specimens. (1 ft-lb = 1.355 J).

XBL8310-6535

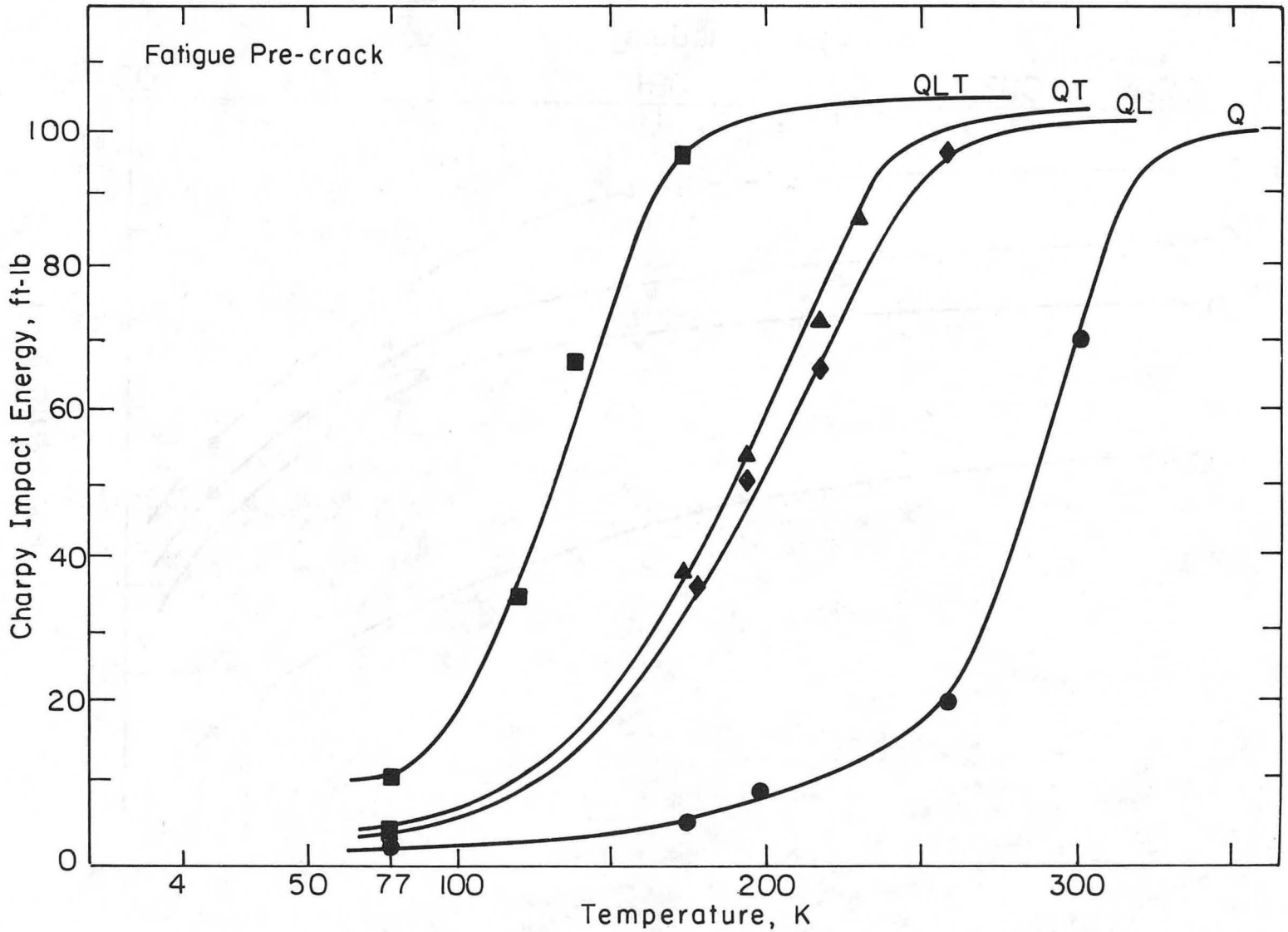

Fig. 25. Ductile-to-Brittle Transition curves as a function of heat treatment for fatigue pre-cracked specimens. (1 ft-lb = 1.355 J).

XBL 8310-6537

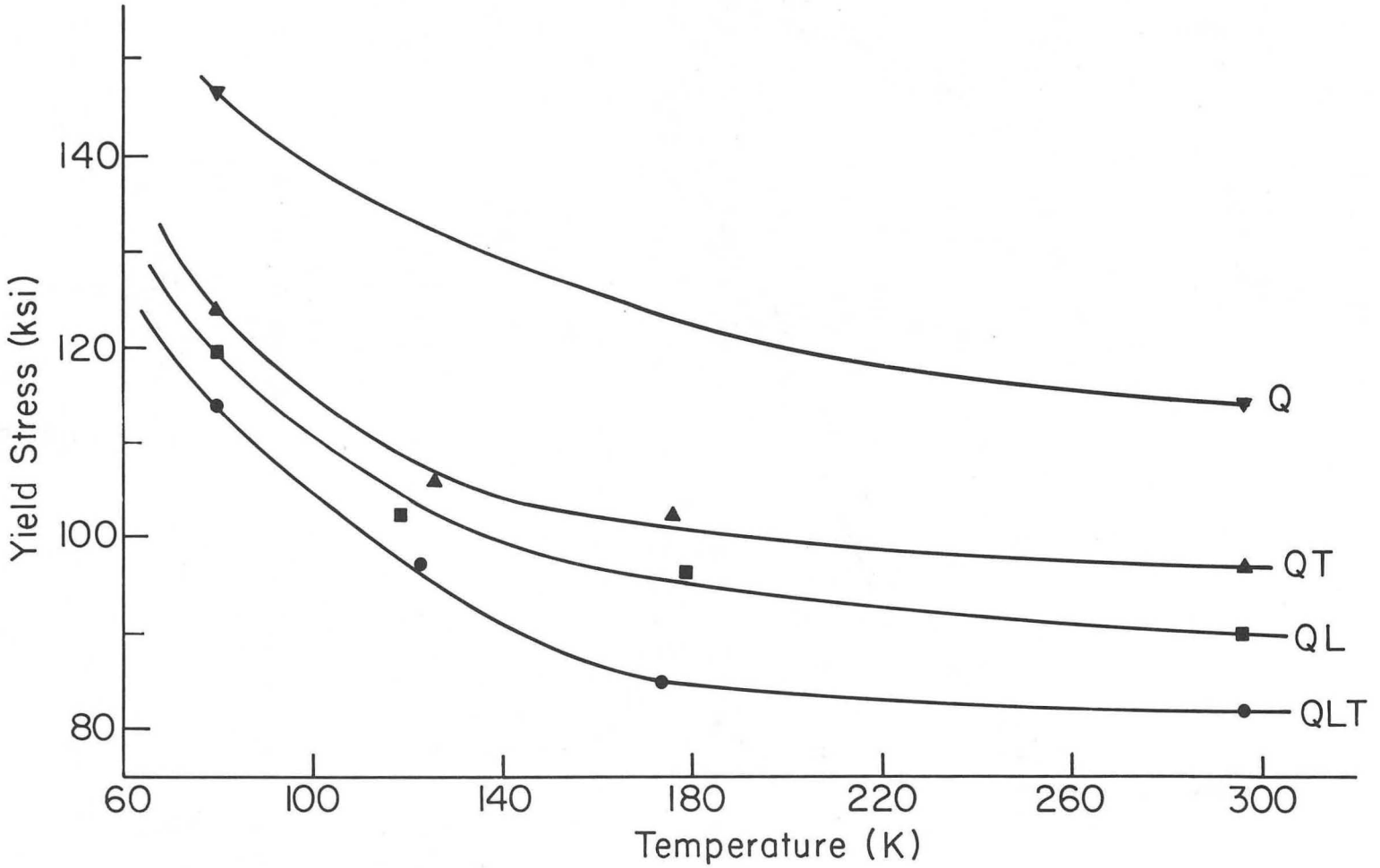

Fig. 26. Yield stress for the various heat treatments as a function of temperature. (1 ksi = 6.89 MPa).

XBL 844-6835

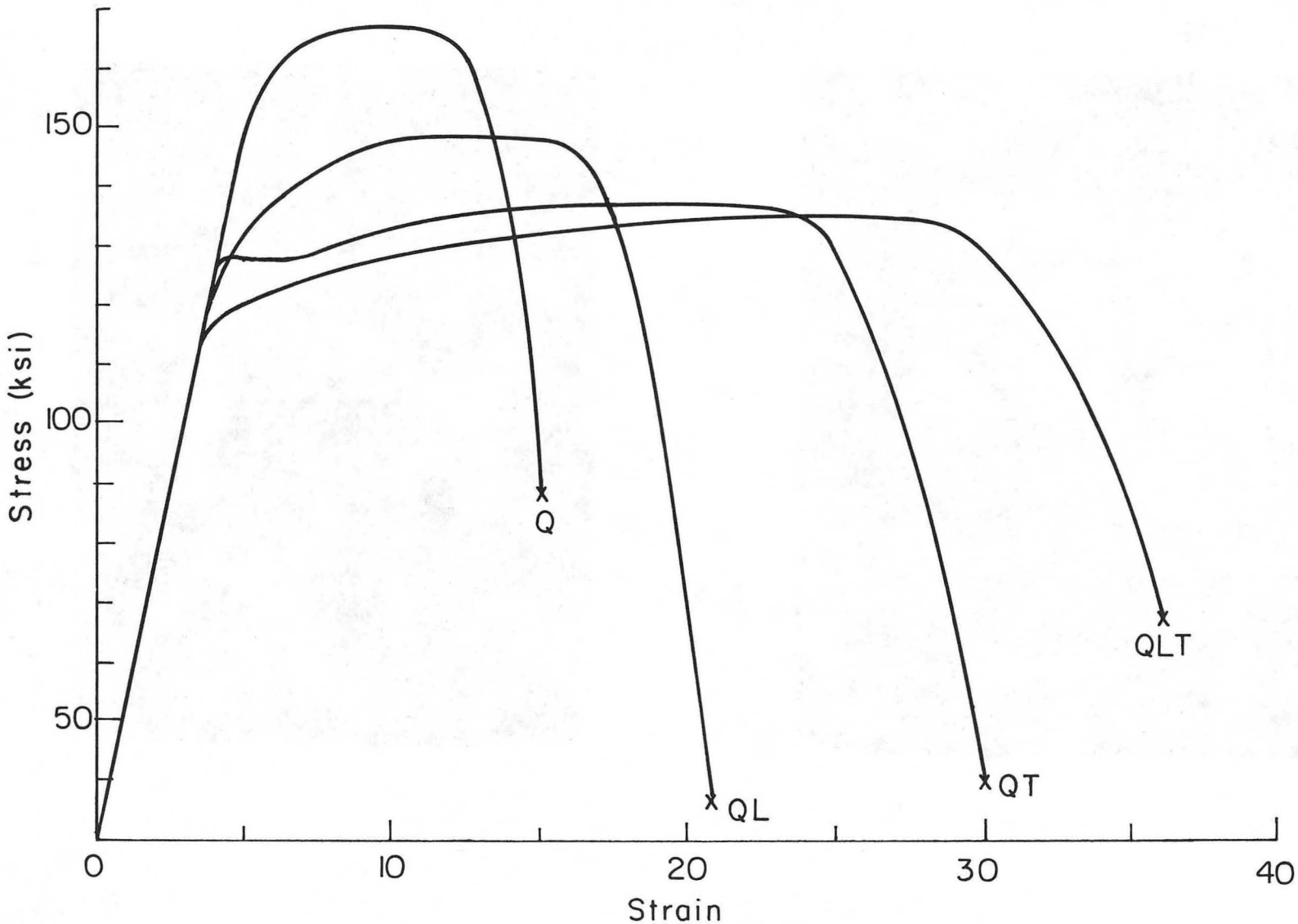

Fig. 27. True stress strain diagrams as a function of heat treatment tested at 77K. (1 ksi = 6.89 MPa).

XBL 844-6840

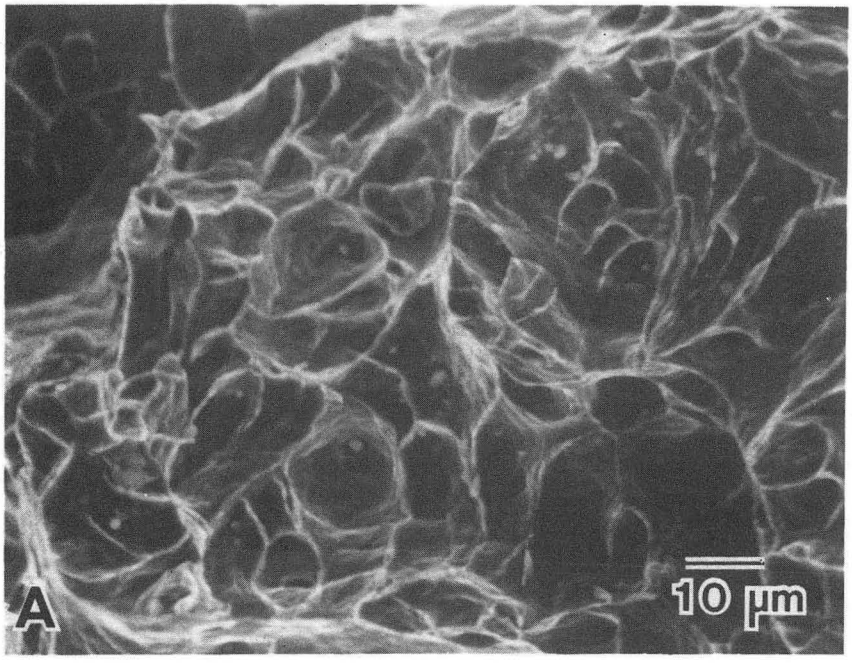

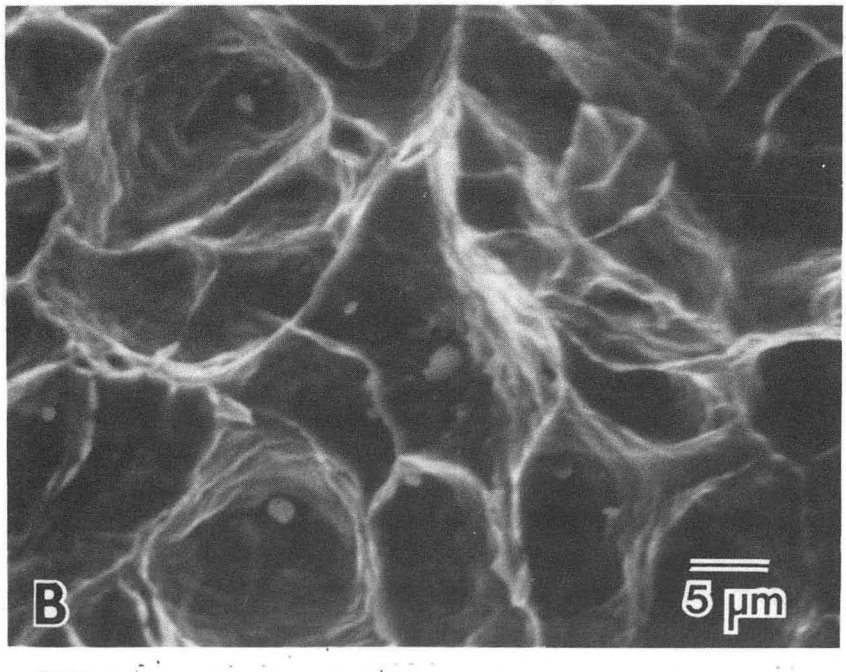

Fig. 28. SEM fractographs of ductile fracture of an Fe-8Ni-2Mn specimen, A)Low magnification B)Higher magnification of A) showing MnS inclusions.

XBB 830-11077

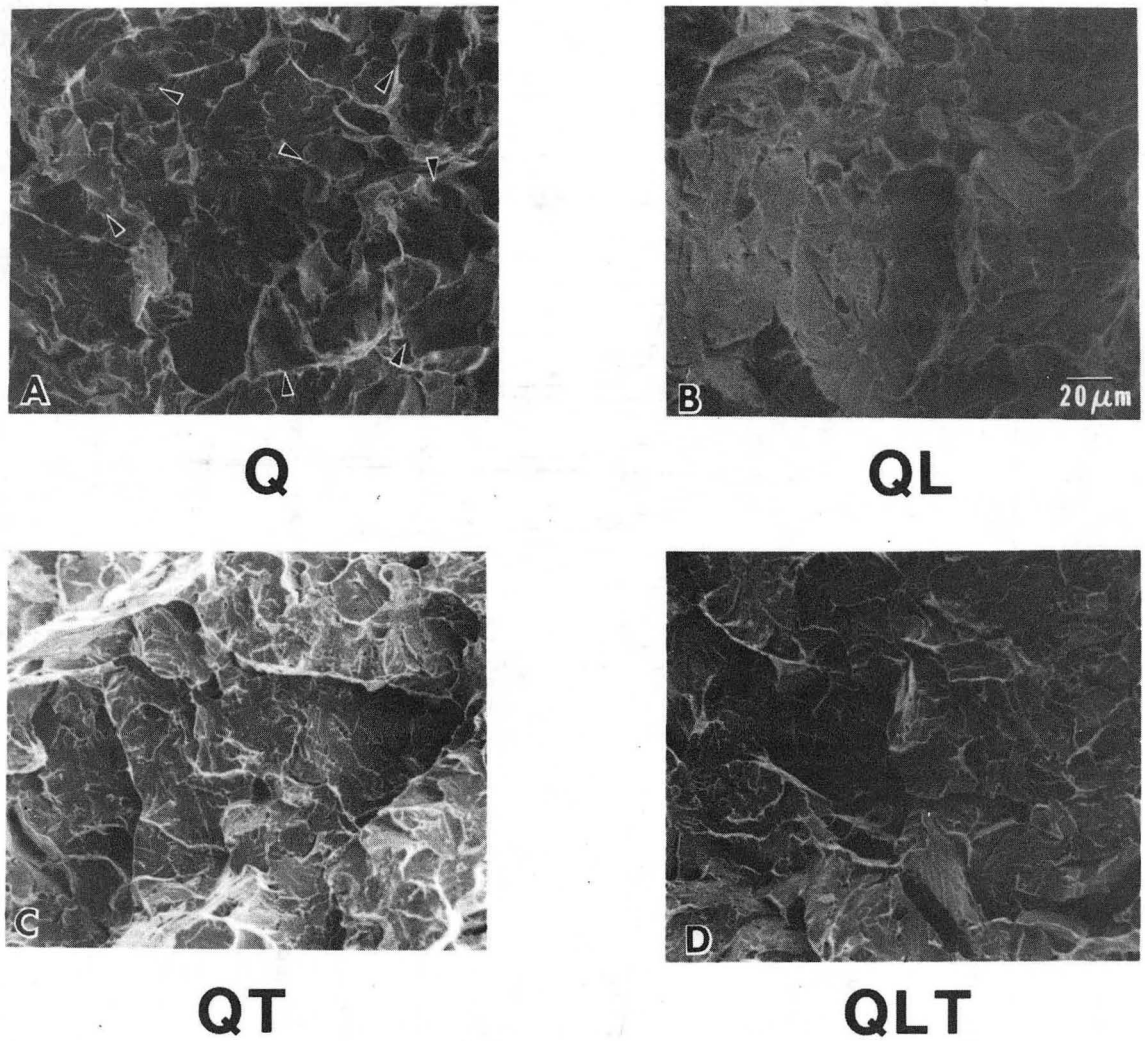

Fig. 29. SEM fractographs of the brittle fracture surfaces as a function of heat treatment.

XBB 830-11091

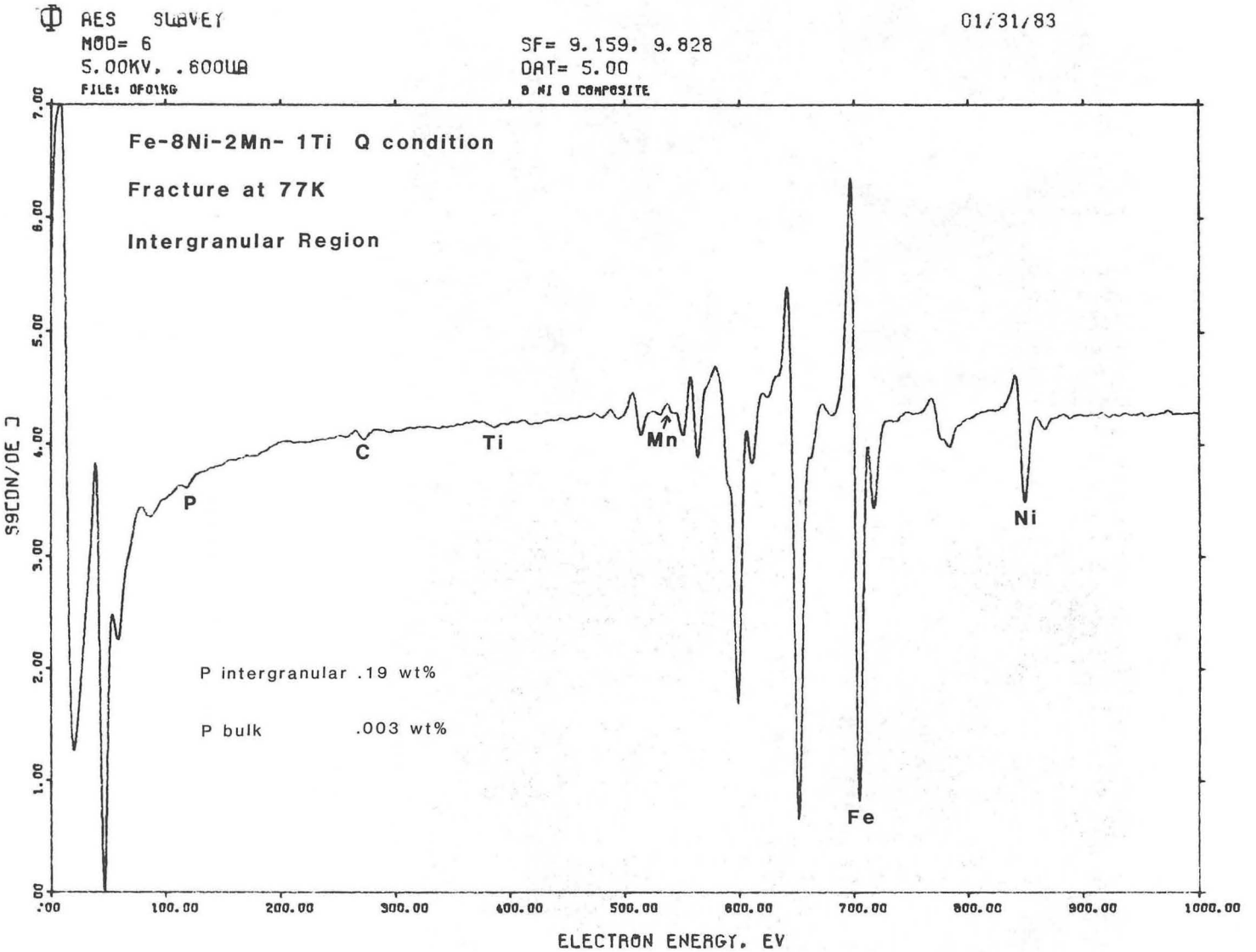

Fig. 30. Auger Electron Spectrum of the brittle intergranular Q specimen.

XBL 844-1439

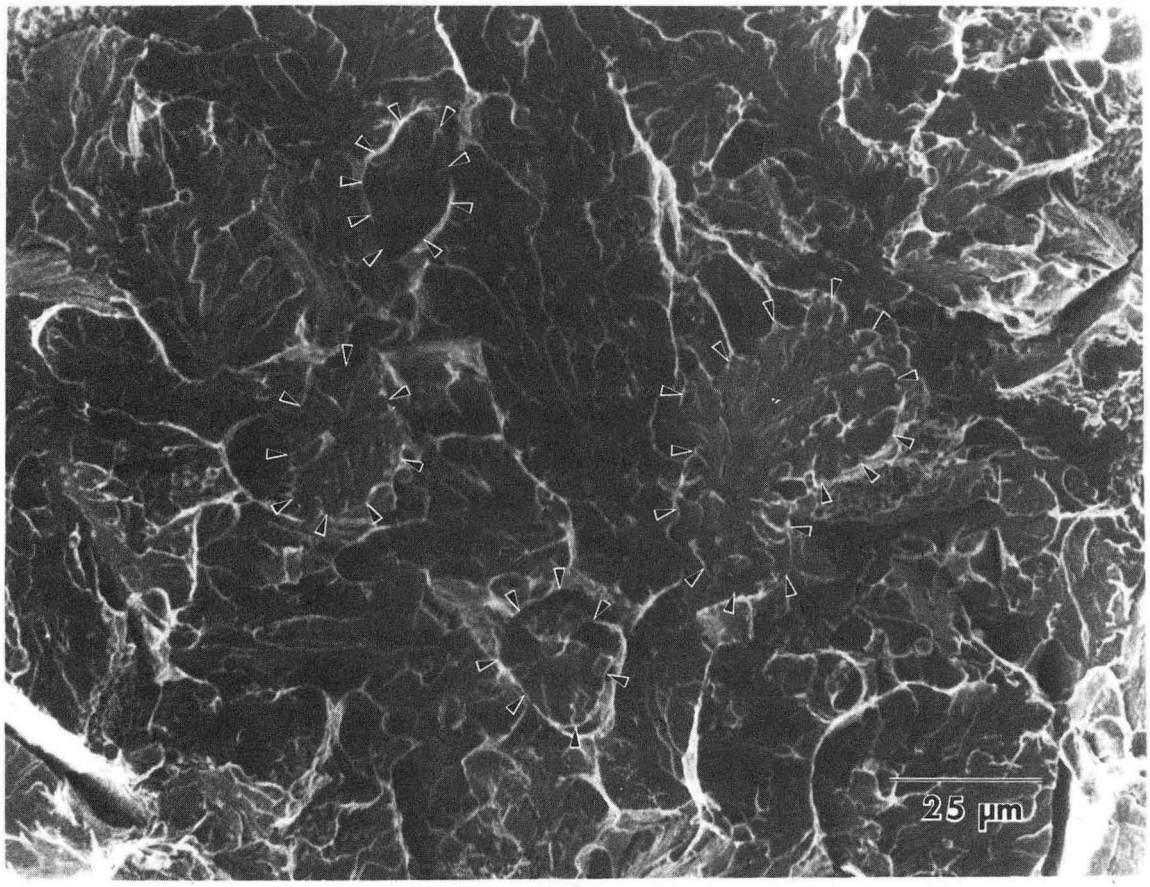

Fig. 31. SEM micrograph of brittle fracture surface with typical facets outlined by arrows.

XBB 844-2632

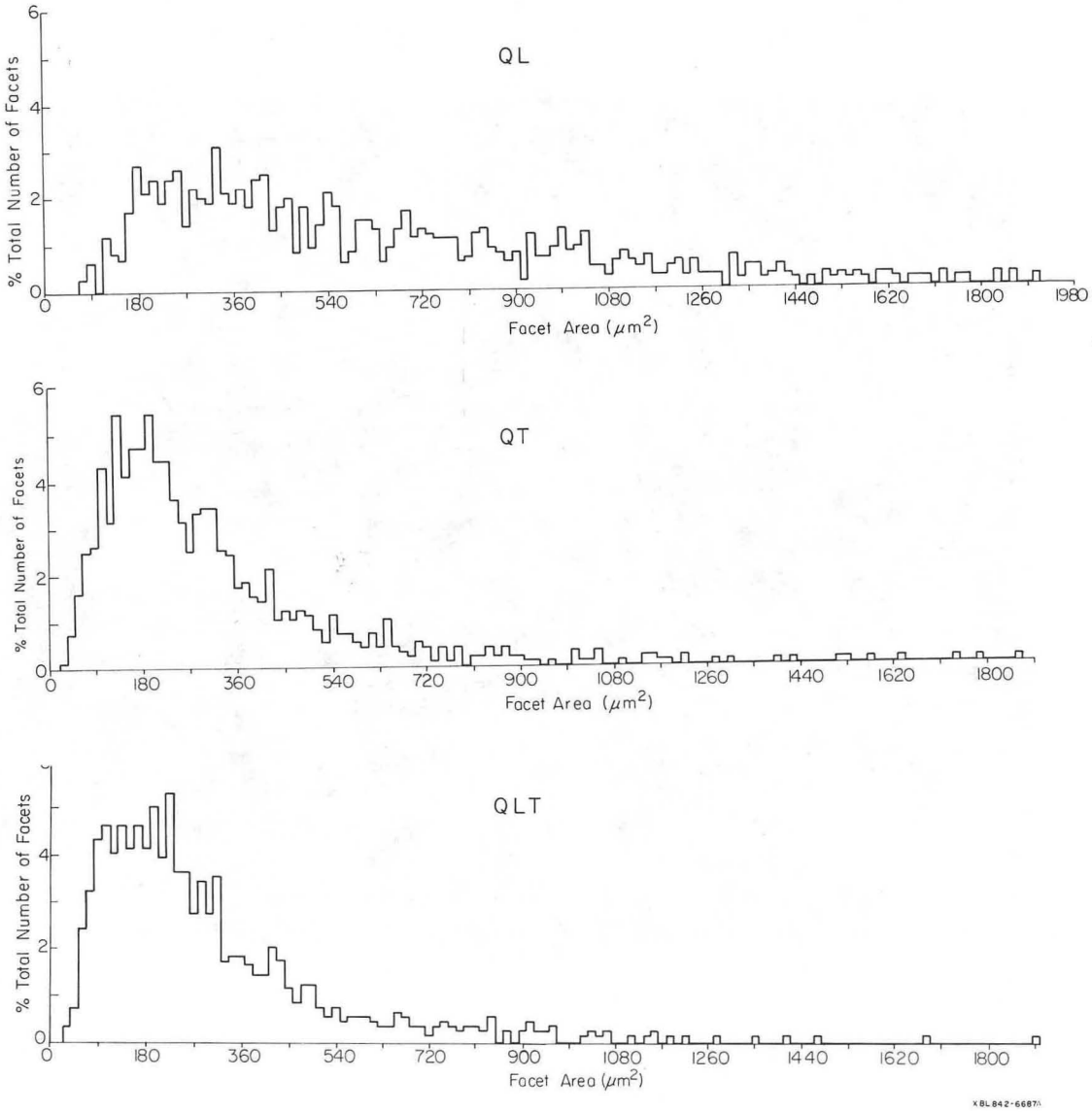

Fig. 32. Histogram plots showing facet size distribution as a function of heat treatment.

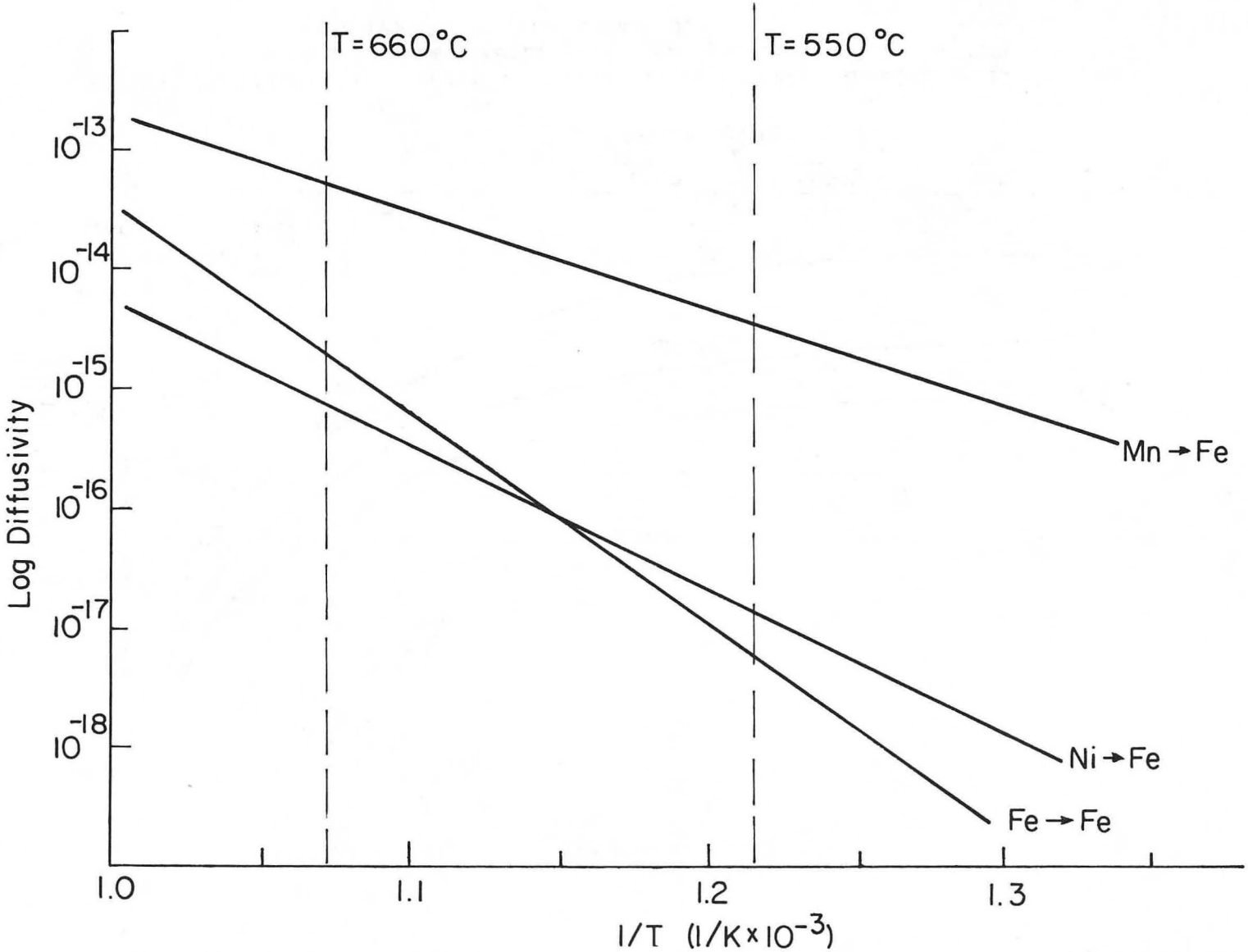

Fig. 33. Arrhenius plot of Diffusivity vs. 1/T showing Mn, Ni, and Fe diffusion in BCC Fe.

XBL 844-6838

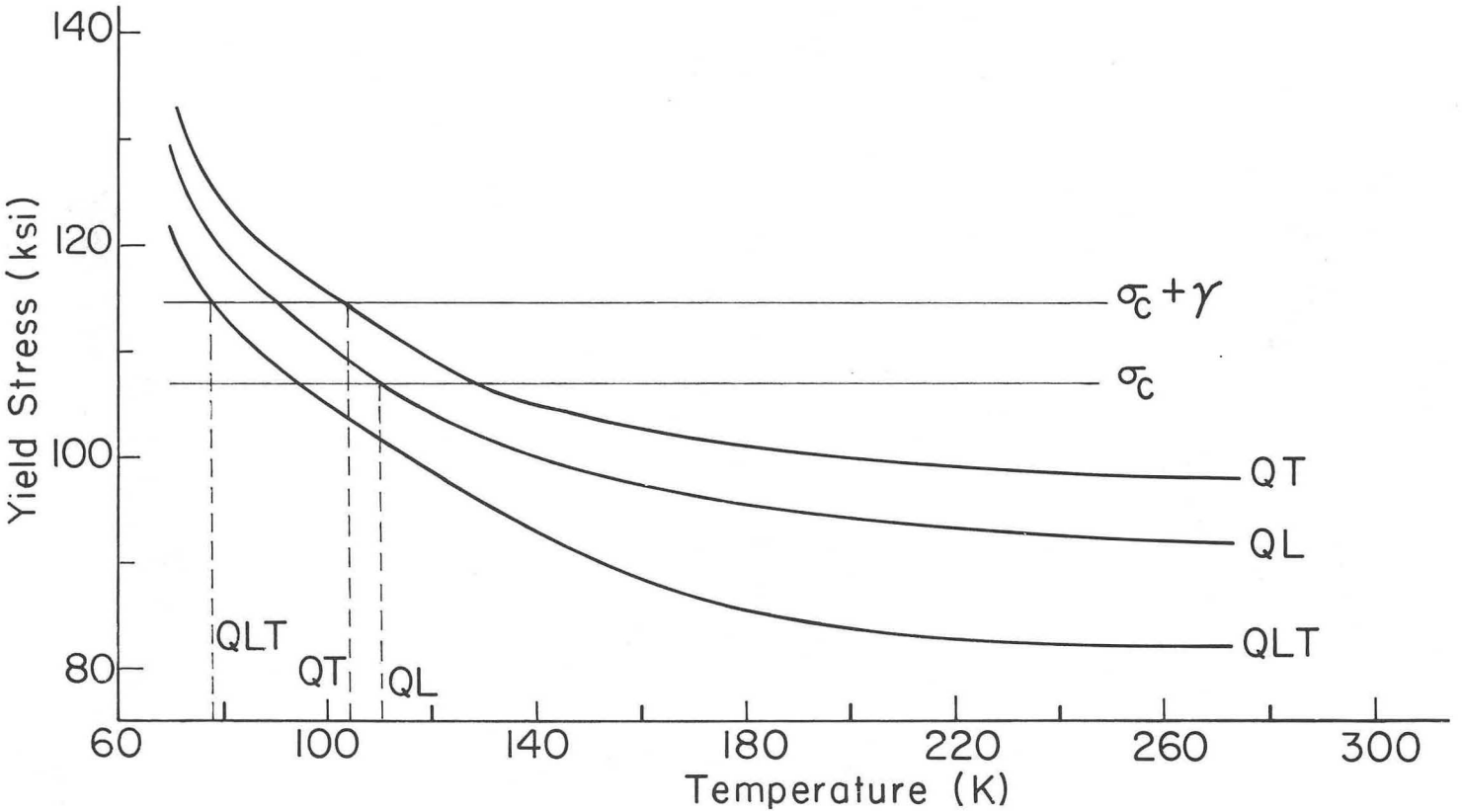

XBL 844-6837

Fig. 34. Schematic diagram of stress vs. temperature showing yield stress and the hypothesized cleavage stress with the DBTT of each heat treatment indicated.

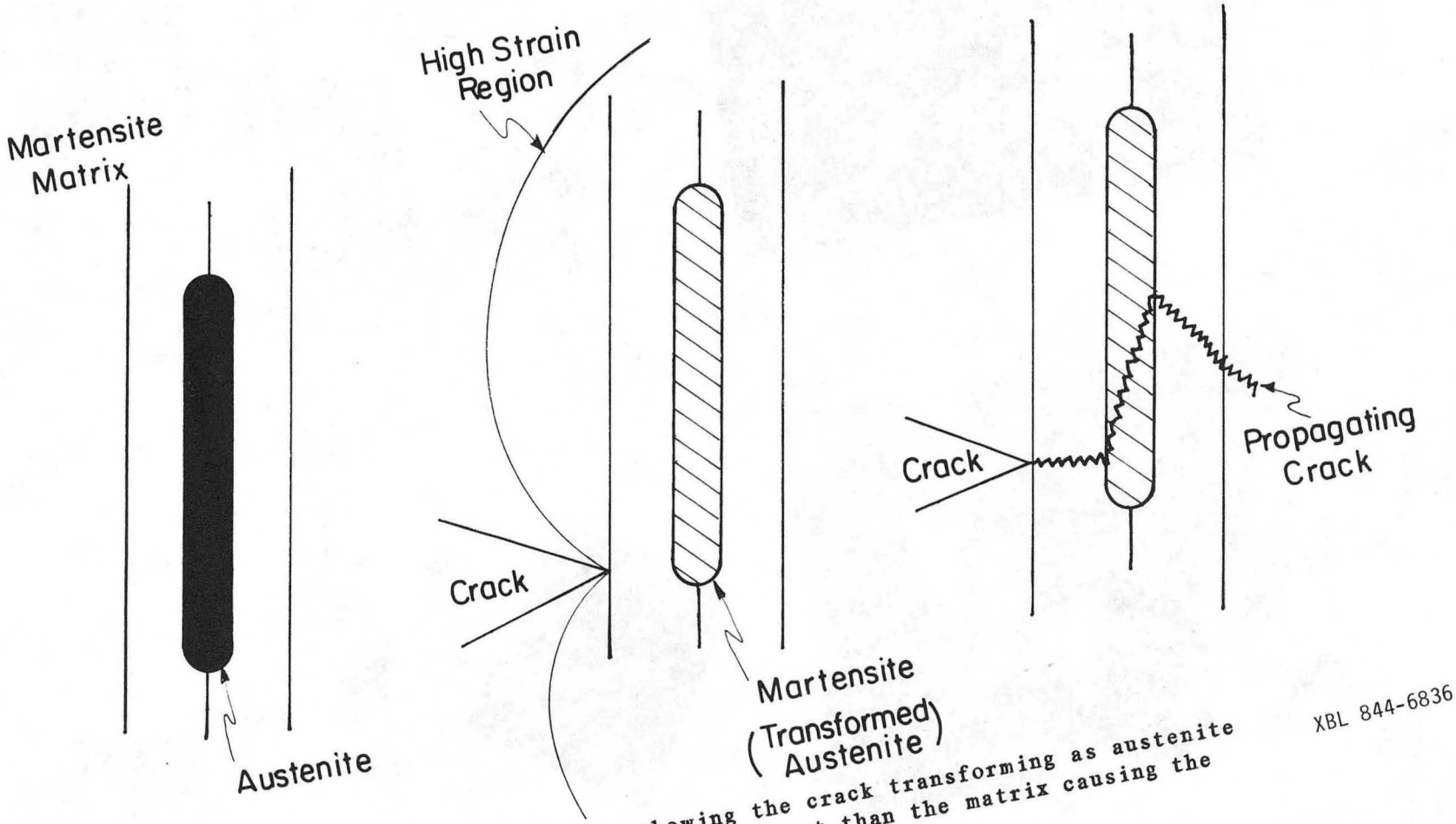

XBL 844-6836

Fig. 35. Schematic diagram showing the crack transforming as austenite particle to a variant different than the matrix causing the crack to hit a high angle boundary.

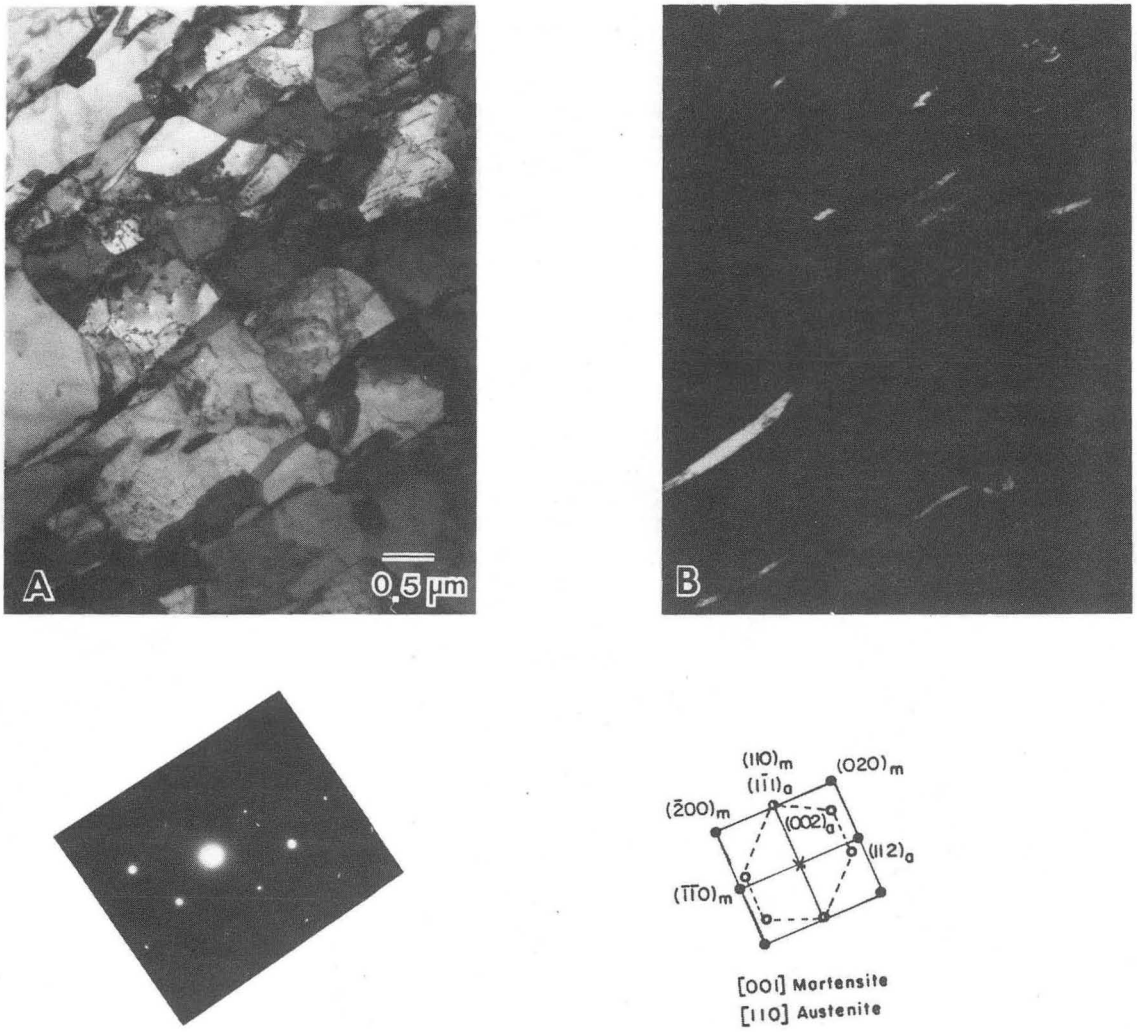

Fig. 36. TEM micrograph of QLT specimen, A)Bright Field image, B)Dark Field contrast showing the distribution of austenite.

XBB 830-11084

This report was done with support from the Department of Energy. Any conclusions or opinions expressed in this report represent solely those of the author(s) and not necessarily those of The Regents of the University of California, the Lawrence Berkeley Laboratory or the Department of Energy.

Reference to a company or product name does not imply approval or recommendation of the product by the University of California or the U.S. Department of Energy to the exclusion of others that may be suitable.

TECHNICAL INFORMATION DEPARTMENT
LAWRENCE BERKELEY LABORATORY
UNIVERSITY OF CALIFORNIA
BERKELEY, CALIFORNIA 94720